© 2019. Published by The Company of Biologists Ltd | Development (2019) 146, dev169482. doi:10.1242/dev.169482

RESEARCH ARTICLE

The intestinal intermediate filament network responds to and protects against microbial insults and toxins

Florian Geisler[1], Richard A. Coch[1], Christine Richardson[2], Martin Goldberg[2], Bernd Denecke[3], Olaf Bossinger[1,*] and Rudolf E. Leube[1,‡]

ABSTRACT

The enrichment of intermediate filaments in the apical cytoplasm of intestinal cells is evolutionarily conserved, forming a sheath that is anchored to apical junctions and positioned below the microvillar brush border, which suggests a protective intracellular barrier function. To test this, we used *Caenorhabditis elegans*, the intestinal cells of which are endowed with a particularly dense intermediate filament-rich layer that is referred to as the endotube. We found alterations in endotube structure and intermediate filament expression upon infection with nematicidal *B. thuringiensis* or treatment with its major pore-forming toxin crystal protein Cry5B. Endotube impairment due to defined genetic mutations of intermediate filaments and their regulators results in increased Cry5B sensitivity as evidenced by elevated larval arrest, prolonged time of larval development and reduced survival. Phenotype severity reflects the extent of endotube alterations and correlates with reduced rescue upon toxin removal. The results provide *in vivo* evidence for a major protective role of a properly configured intermediate filament network as an intracellular barrier in intestinal cells. This notion is further supported by increased sensitivity of endotube mutants to oxidative and osmotic stress.

KEY WORDS: *Caenorhabditis elegans*, *Bacillus thuringiensis*, Endotube, Intermediate filaments, Intracellular barrier function, Pore-forming toxins, Cry5B, Stress

INTRODUCTION

Intestinal epithelia are gatekeepers of two seemingly opposing functions by facilitating uptake of digested nutrients and by providing an efficient barrier to the luminal environment (Baumgart and Dignass, 2002). The intestinal brush border, consisting of closely spaced microvilli, presents a large apical membrane surface that is specialized for selective and effective uptake of food components (Crawley et al., 2014). The barrier function, on the other hand, has been ascribed to tightly regulated cell-cell adhesion complexes that are positioned immediately below the apical membrane domain (Chelakkot et al., 2018; Turner, 2009). Whether and how the arrangement of the junction-associated submicrovillar cytoskeleton contributes to the barrier function is less well understood.

[1]Institute of Molecular and Cellular Anatomy, RWTH Aachen University, 52074 Aachen, Germany. [2]School of Biological and Biomedical Sciences, Department of Biosciences, Durham University, Durham DH1 3LE, UK. [3]Genomics Facility, IZKF Aachen, RWTH Aachen University, 52074 Aachen, Germany.
*Present address: Institute of Anatomy I, Molecular Cell Biology, University of Cologne, 50937 Cologne, Germany.

‡Author for correspondence (rleube@ukaachen.de)

R.E.L., 0000-0002-5519-7379

Received 28 June 2018; Accepted 19 December 2018

The apical cytoplasm of intestinal cells consists of a juxtamembraneous, organelle-free region that is referred to as the terminal web. It is rich in actin, together with proteins that facilitate cytoskeletal cross-linking and membrane attachment including members of the ezrin-moesin-radixin and spectrin families (Bement and Mooseker, 1996). This region is traversed by microvillar actin filament bundles, rootlets of which rest on the underlying intermediate filament (IF)-rich layer in mammals (Bement and Mooseker, 1996; Hirokawa et al., 1982). This layer forms a dense network and is anchored to desmosomal cell-cell junctions (Brown et al., 1983; Franke et al., 1979). A comparable subapical enrichment of desmosome-anchored IFs has been described in adluminal cells of other epithelia, notably in umbrella cells of the urothelium and ciliated cells of the tracheobronchial epithelium (Tateishi et al., 2017; Veranič and Jezernik, 2002), and may reflect a general organizational principle of juxtamembraneous IFs in various cell types (Quinlan et al., 2017).

Moreover, the overall arrangement of the apical cytoplasm is conserved between the mammalian and *Caenorhabditis elegans* intestinal cells. The IF-rich layer is particularly prominent in *C. elegans*, forming an electron-dense sheath-like structure, which separates the apical organelle-free terminal web region from the cytoplasm below, and is attached to the composite *C. elegans* apical junction (CeAJ). It is referred to as the endotube (Munn and Greenwood, 1984). We have recently identified two major endotube regulators: Loss of function mutation of the MAPK orthologue SMA-5 leads to local endotube thickening and disruption, which results in intestinal lumen widening and formation of multiple cytoplasmic invaginations (Geisler et al., 2016), whereas knockout of the intestinal filament organizer IFO-1 (also referred to as TTM-4; Kao et al., 2011) induces complete endotube loss with concurrent formation of large IF protein-containing aggregates at the CeAJ and in the cytoplasm (Carberry et al., 2012). Six IF polypeptides are presumably localized in the endotube: IFB-2, IFC-1, IFC-2, IFD-1, IFD-2 and IFP-1, encompassing several splice variants (reviewed by Carberry et al., 2009).

Multiple functions have been ascribed to the IF-rich endotube in *C. elegans* and the orthologous layer in intestinal epithelia of other organisms. Most attention has been paid to its contribution in establishing and maintaining epithelial polarity (reviews by Coch and Leube, 2016; Salas et al., 2016). Furthermore, it has been suggested that this subapical IF network provides mechanical resilience and plasticity, although direct experimental evidence is still lacking (Geisler et al., 2016; Hüsken et al., 2008; Jahnel et al., 2016). And finally, it has been proposed that the dense layer of IFs below the terminal web acts as a barrier against extracellular stressors, protecting especially against microbial insults (review by Geisler and Leube, 2016). Although specific microbe-IF interactions have been described in various paradigms (Geisler and Leube, 2016), the overall protective function of the

Development (2019) 146, dev169482. doi:10.1242/dev.169482

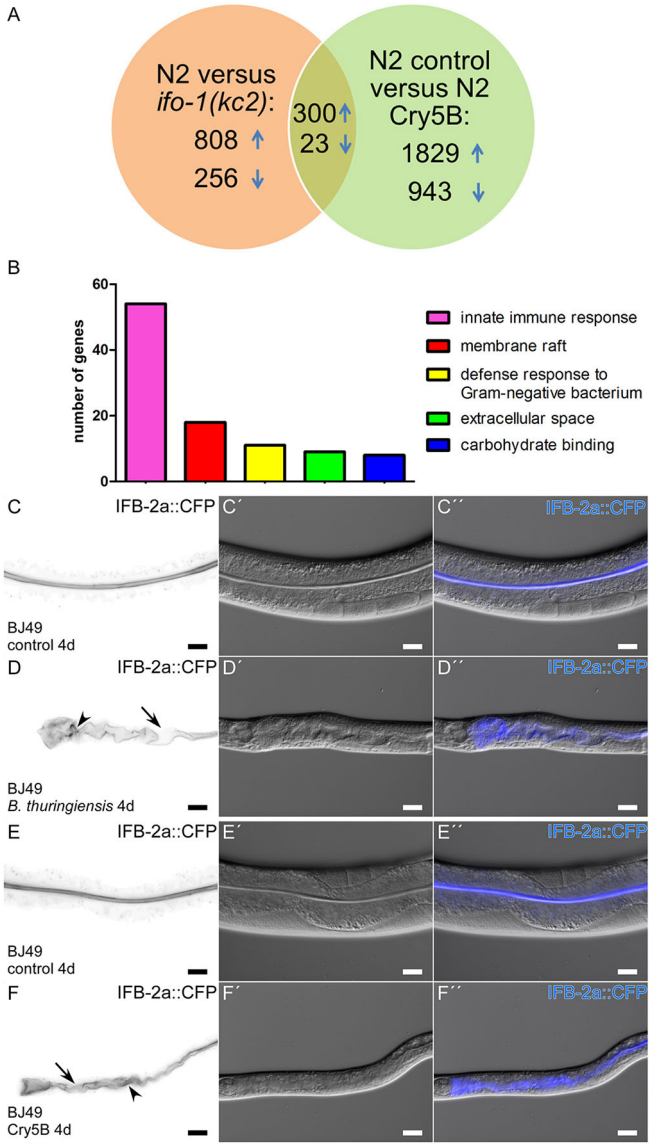

Fig. 1. Endotube mutants share changes in gene expression with Cry5B-intoxicated worms, which, similar to *B. thuringiensis*-infected worms, present structural endotube changes. (A,B) mRNA levels were analyzed in triplicates either in dissected intestines of L4 *ifo-1(kc2)* versus N2 grown on OP50 control bacteria, or in N2 grown on Cry5B-producing JM103 versus N2 grown on control JM103. Changes in mRNA expression were scored as significant with a fold change of >2 and a *P*-value <0.05. Venn diagram showing the number of genes that were upregulated and downregulated in each situation, or co-regulated in both paradigms (overlap) (A). Histogram derived from ontology analyses of the co-regulated genes (Table S3) presenting the most affected biological processes (innate immune response, defense response to Gram-negative bacterium), cellular compartments (membrane raft, extracellular space) and metabolic function (carbohydrate binding) (B). The respective genes are listed in Table S4. (C-F″) The *in vivo* images show the distribution of fluorescent IF protein IFB-2a::CFP, which specifically labels the endotube (C-F; C′-F′ show corresponding interference contrast images; C″-F″ show merged images). Animals were grown for 4 days after hatching on OP50 (C-C″), *B. thuringiensis* strain DB27 (D-D″), control JM103 (E-E″) and Cry5B-producing JM103 (F-F″). Animals grown on either control bacteria reach adulthood and displayed a smooth periluminal IFB-2a::CFP localization in the intestine (C-C″, E-E″) as is typical for a fully developed endotube. In contrast, infection with *B. thuringiensis* DB27 (D-D″) or intoxication with the pore-forming toxin Cry5B (F-F″) induce intestinal lumen dilation and formation of multiple cytoplasmic invaginations of the IF-rich endotube (compare C,C′ with D,D′ and E,E′ with F,F′). Note also the heterogeneities of reporter fluorescence with local loss of fluorescence (arrows) and local fluorescence enrichment (arrowheads) in the infected and intoxicated intestines (D,F). Scale bars: 20 µm.

subapical intestinal IF network has not been examined systematically.

The goal of the current study was therefore to investigate whether and how the IF-rich endotube protects against microbial insults. We decided to use *Bacillus thuringiensis* infection as a well-established model to study microbe-host interactions in *C. elegans* (e.g. Iatsenko et al., 2013; Rae et al., 2010; Rae et al., 2012; Sifri et al., 2005). The virulence of *B. thuringiensis* is, in large part, determined by pore-forming toxins (e.g. Kho et al., 2011; Marroquin et al., 2000; Wei et al., 2003). By using the previously characterized *sma-5* and *ifo-1* mutants we present evidence that endotube perturbations increase the sensitivity to *B. thuringiensis* and its major pore-forming toxin crystal protein Cry5B. We further show that Cry5B intoxication alters endotube structure. Concurrently, Cry5B elicits responses in IF protein expression and, conversely, depletion of IF protein IFB-2 leads to increased larval arrest and increased time of development in the presence of Cry5B. Examining the responses of the mutant strains to oxidative and osmotic stress further support the notion that the subapical intestinal IF system provides an important intracellular barrier against different challenges.

RESULTS

Mutation of the intestinal filament organizer IFO-1 and Cry5B intoxication induce transcription of a common set of innate immune response genes

As *ifo-1* gene expression has been identified as a target of bacterial toxins (Kao et al., 2011), transcriptome analyses were performed on intestines that had been dissected from endotube-deficient *ifo-1* mutants to identify cellular properties that are regulated by IFO-1. RNA was extracted in triplicate from isolated intestines of either wild-type or *ifo-1(kc2)*-mutant L4 larvae for gene chip analysis (Fig. 1A). It was found that 808 genes were upregulated and 256 genes were downregulated in *ifo-1(kc2)* with a $P<0.05$ (Table S1), and 153 genes were differentially regulated with a *P*-value <0.001. Of those, 68 are annotated as being expressed in the intestine (WormExp; Yang et al., 2016). The *de novo* expression of the remaining genes is either because of the induction of *ifo-1*-dependent pathways or contamination during intestinal microdissection. Interestingly, the expression of the IF-encoding gene *ifd-2* was upregulated 2.66-fold. Gene ontology analyses revealed that membranes were the most affected cellular compartment (261 genes) and that most altered metabolic functions included transferase activity (46 genes) and carbohydrate binding (36 genes). Among regulated biological processes, innate immune response was number one (78 genes). The latter finding suggested that endotube impairment is linked to reduced microbial protection and therefore triggers an innate immune response even in the presence of only mildly pathogenic microbes such as OP50 (Alper et al., 2007).

To compare how the observed changes relate to the physiological response of wild-type worms to microbial stress, RNA was analyzed from N2 treated with Cry5B, the major pathogenic pore-forming toxin of *B. thuringiensis*. To this end, N2 were grown for 4 days on JM103 bacteria that produced Cry5B and control JM103. The subsequent gene chip analyses of L4/young adult worms identified 1829 genes that were upregulated and 943 genes that were downregulated upon Cry5B intoxication (Fig. 1A; Table S2). Ontology analyses showed that the nucleus and cytoskeleton were

Development (2019) 146, dev169482. doi:10.1242/dev.169482

the most affected cellular compartments (233 and 55 genes, respectively) and that ATP binding was the most affected metabolic function (142 genes). Remarkably, and in accordance with previous analyses (Huffman et al., 2004; Kao et al., 2011), the most affected biological process was innate immune response (149 genes). Of note, the non-intestinal IF protein-encoding gene *ifa-3* was downregulated 7.04-fold, whereas the intestinal IF protein-encoding gene *ifd-2* was upregulated 4.01-fold. As a caveat, we would like to stress, however, that the differential gene expression of Cry5B-treated worms is in part due to developmental arrest.

Be that as it may, comparison of altered mRNA expression in *ifo-1(kc2)* and in Cry5B-intoxicated N2 identified 300 candidates that were upregulated and 23 that were downregulated in both situations (for complete list see Table S3). Of those, 54 genes are related to the innate immune response (52 upregulated and two downregulated) and 11 genes are related to the defense response to Gram-negative bacteria (10 upregulated and one downregulated). Membrane rafts (18 upregulated genes) and extracellular space (eight upregulated and one downregulated genes) were the most affected cellular compartments, and carbohydrate binding (eight upregulated genes) was the most altered metabolic function (Fig. 1B, Table S4).

Taken together, we take the above observations as an indication for a link between the impaired endotube and reduced microbial protection in *ifo-1* mutants triggering an innate immune response even in the absence of enhanced microbial stress.

B. thuringiensis and its pore-forming toxin Cry5B induce structural alterations of the intermediate filament-rich endotube

To find out whether and how endotube alterations occur during *B. thuringiensis* infection and/or Cry5B intoxication, we employed strain BJ49 for monitoring endotube changes in living animals. BJ49 contains an integrated array encoding fluorescent IFB-2 reporter IFB-2a::CFP (Hüsken et al., 2008). Adult BJ49 grown on standard OP50 bacteria presented a subapically enriched fluorescence that surrounded the microvillar brush border of the evenly shaped ellipsoid intestinal lumen (Fig. 1C-C″). Placing BJ49 larvae on *B.thuringiensis* strain DB27, however, led to overall growth retardation. The intestine became considerably altered, with extensive luminal widening and formation of multiple cytoplasmic invaginations surrounded by IFs that were less evenly distributed, presenting local accumulations and gaps (Fig. 1D-D″).

To exclude that the phenotype is affected by overexpression of the integrated IFB-2a::CFP transgene and to find out whether other IF polypeptides also redistribute upon DB27 infection, we studied knock-in worms containing *ifc-2* allele *kc16*, which encodes fluorescent reporter IFC-2a::YFP. Fig. S1A-B″ illustrates that luminal widening, cytoplasmic invaginations and heterogeneities of fluorescence were also discernable in the intestine of *B. thuringiensis*-infected worms.

To see whether the pore-forming toxin Cry5B elicits similar changes in the intestine as DB27, worms were placed on JM103 *Escherichia coli* strain that produced Cry5B. The resulting luminal widening, cytoplasmic invaginations and endotube heterogeneities (compare Fig. 1E-E″ and Fig. S1C-C″ with Fig. 1F-F″ and Fig. S1D-D″, respectively) were readily apparent. As the alterations were indistinguishable from those detected in the intestine of DB27-infected worms, subsequent studies were performed with Cry5B-producing JM103 and control JM103 bacteria that contained only the empty pQE9 vector backbone.

Propidium iodide incubation demonstrated that Cry5B intoxication induced loss of apical membrane integrity, whereas paracellular spaces remained inaccessible, which indicated functional maintenance of the *C. elegans* apical junction (Fig. S2). Electron microscopy was done next to further characterize Cry5B-induced ultrastructural changes in the intestine. Fig. 2A shows the intestine of N2 after 3 days growth on control JM103, presenting the typical subapical localization of the electron-dense endotube sandwiched between the electron-lucent terminal web region and the cytoplasm below, serving as anchorage for microvillar actin filament bundles. As Cry5B intoxication caused considerable growth retardation, phenotypic changes were examined only after 4 days. The resulting phenotypes differed between worms and even within the intestine of individual worms. In some worms, the brush border still seemed to be mostly intact. But overall thickening of the endotube was visible in these examples (Fig. 2B,C). Occasionally, invaginations were visible (Fig. 2D). In some worms, microvilli were shortened because of massive shedding of microvillar tips into the intestinal lumen (Fig. 2E,F). The microvillar actin bundles, however, were still intact

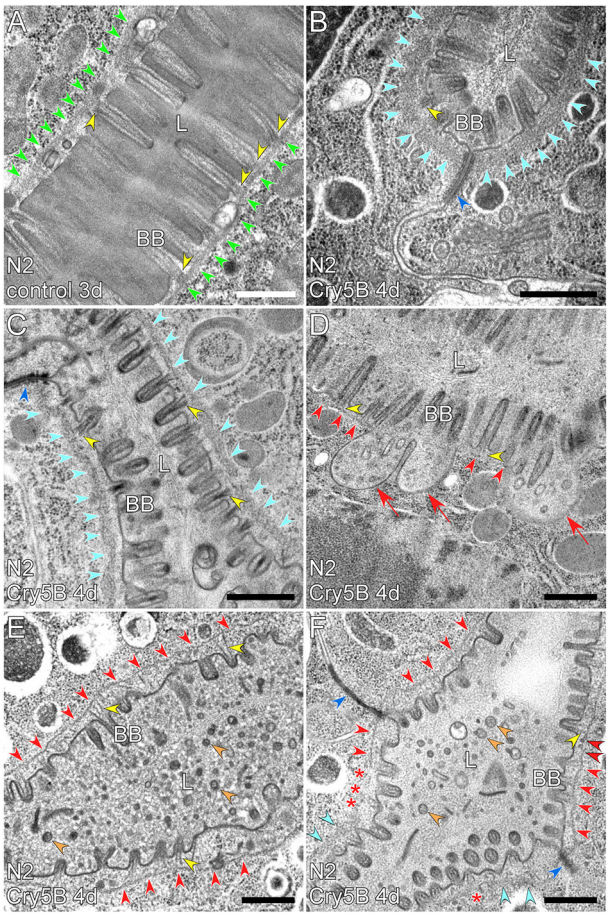

Fig. 2. Wild-type larvae treated with pore-forming Cry5B toxin present luminal perturbation, shortened microvilli and severe endotube alterations. (A-F) Electron micrographs showing sections of N2 larvae that had been fed either with control JM103 for 3 days (A) or with Cry5B-producing JM103 for 4 days (B-F). B-C depict increased endotube width (light blue arrowheads) compared with the control (green arrowheads in A), although the brush border (BB) is still unperturbed. D-F show regions of other worms with invaginations (red arrows in D), rarefied endotubes (red arrowheads), localized thickening (light blue arrowheads) and local gaps (red asterisks in F). Note also the shortened, irregular microvilli in E and F, which are, however, still anchored to the endotube through actin bundles (compare yellow arrowheads in B-F with A) traversing the enlarged, organelle-free terminal web. A dilated lumen (L) with abundant cellular debris containing shed microvillar tips (orange arrowheads) is seen in E and F. The normal-appearing *C. elegans* apical junctions are marked by dark blue arrowheads in B,C and F. Scale bars: 500 nm.

Development (2019) 146, dev169482. doi:10.1242/dev.169482

in the remaining microvilli protruding into the apical cytoplasm (Fig. 2E,F). They traversed a widened terminal web region and were anchored to the endotube. The endotube was a lot thinner in regions with massive loss of microvilli (Fig. 2E,F). In some regions the endotube even became discontinuous with local gaps (Fig. 2F). Junctional morphology was inconspicuous throughout (Fig. 2B,C,F).

Cry5B elicits re-distribution of the endotube regulators SMA-5 and IFO-1

As we have previously shown that the MAPK orthologue SMA-5 and the intestinal filament organizer IFO-1 act as regulators of endotube formation (Carberry et al., 2012; Geisler et al., 2016), we wanted to know whether they are affected by Cry5B intoxication. To monitor changes in SMA-5 distribution, we used the SMA-5::EGFP-producing reporter strain BJ263 (Geisler et al., 2016). Cry5B intoxication led to a redistribution of the pan-cytoplasmic diffuse fluorescence into dot-like structures, which may correspond to cytoplasmic vesicles (Fig. 3A-B′). Of note, this phenotype could also be elicited by treating animals with *ifo-1(RNAi)* in the absence of any toxin (Fig. S3).

To study IFO-1 distribution, we used IFO-1::YFP-producing strain BJ186 (Carberry et al., 2012). Fluorescence microscopy revealed that most IFO-1 was still localized in the subapical domain following exposure to Cry5B, but was reduced in some places, with increased diffuse cytoplasmic fluorescence compared with the control (Fig. 3C-D′). Together, these observations suggest that SMA-5 and IFO-1 are involved in development of the Cry5B-mediated endotube pathology.

sma-5 and *ifo-1* mutant strains are hypersensitive to Cry5B intoxication

In this set of experiments, we wanted to explore how SMA-5-dependent endotube weakening and IFO-1-dependent endotube disruption affect the sensitivity to Cry5B intoxication. To this end, *sma-5(n678)* deletion mutant and *ifo-1(kc2)* point mutant, both of which result in functional knockout (Carberry et al., 2012; Watanabe et al., 2005), were grown either on Cry5B-producing JM103 or control JM103 bacteria. As expected, larval arrest was not observed on control bacteria for N2 (0%) but was detected in worms carrying allele *n678* (13.89%) and *kc2* (9.59%; Fig. 3E). None of the larvae that were scored as ‘arrested’ developed into adulthood,

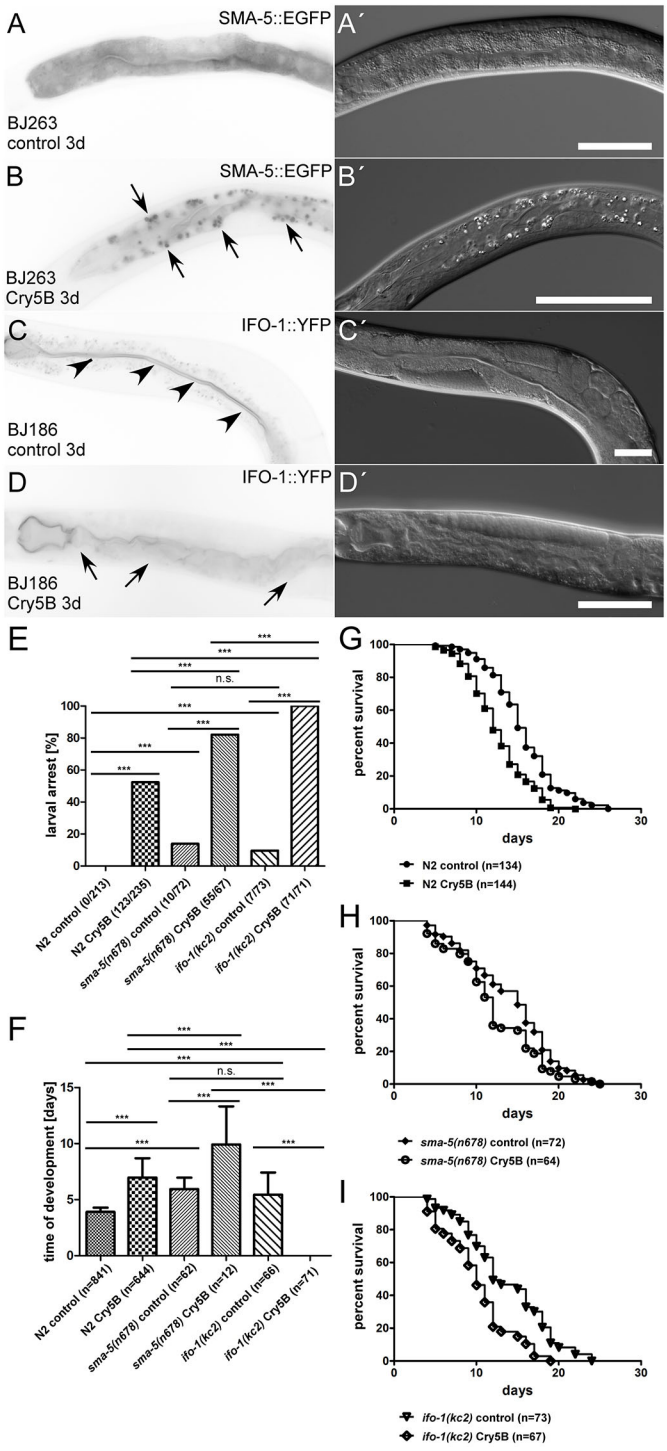

Fig. 3. Cry5B intoxication induces re-distribution of major endotube regulators and leads to increased larval arrest, increased time of development and shortened lifespan. (A-D′) *In vivo* images obtained from animals that expressed either SMA-5::EGFP (A,B; corresponding interference contrast images in A′,B′) or IFO-1::YFP (C,D; corresponding interference contrast images in C′,D′). Animals were grown for 3 days after hatching either on control JM103 (A,A′,C,C′) or on Cry5B-producing JM103 (B,B′,D,D′). Note that SMA-5::EGFP re-distributes to a punctate ‘vesicular’ compartment in the cytoplasm (arrows in B) and that the typical periluminal localization of IFO-1::YFP (arrowheads in C) is replaced by increased diffuse cytoplasmic fluorescence and discontinuous apical localization (arrows in D). Scale bars: 50 µm. (E) N2 grown on control JM103 have no larval arrest (n=0/213), whereas 52.34% of Cry5B-intoxicated animals arrest during larval development (n=123/235, P<0.0001). Mutants with impaired endotubes already show mild larval arrest under control conditions [*sma-5(n678)*: 13.89%, n=10/72; *ifo-1(kc2)*: 9.59%, n=7/73] and Cry5B treatment leads to a massive increase of larval arrest [*sma-5(n678)*: 82.09% (n=55/67); *ifo-1(kc2)*: 100% (n=71/71), P<0.0001]. (F) Note that the time of development is increased in Cry5B-intoxicated wild-type animals (N2 control: 3.91±0.37 days, n=841, versus N2 Cry5B: 6.97±1.72 days, n=644; P<0.0001). In comparison with the wild type, *sma-5(n678)* and *ifo-1(kc2)* mutants present prolonged time of development when grown on control bacteria [*sma-5(n678)*: 5.94±1.02 days, n=62; *ifo-1(kc2)*: 5.44±1.98 days, n=66; P<0.0001]. Treatment of *sma-5(n678)* with Cry5B increases time of development even more (9.92±3.40 days, n=12; P<0.0001). Note that measurements in *ifo-1(kc2)* are not possible because of the full larval arrest (see E; n=71). (G-I) Survival data as plots of the Kaplan–Meier estimator. The lifespan of wild-type animals grown on Cry5B-producing bacteria is 3 days shorter than on control bacteria (Cry5B: 12 days, n=144; control: 15 days, n=134; P<0.0001). Mutants with endotube impairment grown on Cry5B-producing bacteria display the same or higher lifespan reduction as the wild type [*sma-5(n678)* control: 15 days, n=72; *sma-5(n678)* Cry5B: 12 days, n=64, P=0.0406; *ifo-1(kc2)* control: 12 days, n=73; *ifo-1(kc2)* Cry5B: 10 days, n=67; P<0.0001]. Larval arrest rates (%) were calculated from the ratios of animals dying as larvae and as adults. Data are mean±s.d.; ***P<0.0001. n.s., not significant.

Development (2019) 146, dev169482. doi:10.1242/dev.169482

with *kc2* mutants arresting at L3 and *n678* mutants developing slightly further. Cry5B intoxication resulted in 52.34% larval arrest in N2 and considerably increased arrest in *n678* (82.09%), with arrest reaching 100% in *kc2*. Intermediate larval stages were observed but could not be unequivocally defined because of multiple developmental defects that resulted in altered gonad development and body size, both of which are important criteria for classical staging. Defects appeared to be more pronounced in *kc2* than in *n678* (see e.g. Fig. 4D,H). Whereas all *kc2* larvae remained at an L1/L2-like stage, wild-type and *n678* larvae developed occasionally into L4-like stages. Similarly, *ifo-1* allele *kc3* (Carberry et al., 2012) also displayed an increased larval arrest in the presence of Cry5B in comparison with the wild type [N2 control: 0% (0/40) versus N2 Cry5B: 57.50% (23/40), $P<0.0001$; *ifo-1(kc3)* control: 31.65% (25/79) versus *ifo-1(kc3)* Cry5B: 95.00% (76/80), $P<0.0001$; N2 control versus *ifo-1(kc3)* control, $P<0.0001$; N2 Cry5B versus *ifo-1(kc3)* Cry5B, $P<0.0001$].

Assessment of larval development (Fig. 3F) revealed that Cry5B intoxication of N2 resulted in developmental retardation (6.97±1.72 versus 3.91±0.37 days; data are mean±s.d.). In *sma-5(n678)*, time of larval development was already slowed down on control JM103 (5.94±1.02 days) and was further increased on Cry5B (9.92 ±3.40 days). Because of the 100% larval arrest of *ifo-1(kc2)* no measurements were possible for Cry5B intoxication in this example. But time of development was also slowed down on control JM103 in comparison with N2 (3.91±0.37 versus 5.44± 1.98 days). Similar results were obtained for *ifo-1(kc3)* animals. Larval development was already retarded in the absence of toxin (N2 control: 4.03±0.01 days, $n=284$ versus *ifo-1(kc3)* control: 6.86±0.13 days, $n=85$, $P<0.0001$) and only very few *ifo-1(kc3)* larvae reached adulthood in the presence of Cry5B, with a dramatic increase in time of development compared with N2 (N2 Cry5B: 7.25±0.14 days, $n=122$ versus *ifo-1(kc3)* Cry5B: 10.75±1.32 days, $n=4$, $P<0.0001$).

Finally, we determined lifespan (Fig. 3G-I) and found that Cry5B intoxication reduced survival of N2 by 3 days (12 days versus 15 days). However survivors, which reach adulthood, remain small. They have severely reduced progeny and frequently present a 'bag of worms' phenotype. Lifespan of *sma-5(n678)* on control bacteria was similar to the wild type (15 days) and was reduced by 3 days upon Cry5B intoxication (12 days). The most severe effects were observed for *ifo-1(kc2)*, whose lifespan on control JM103 was 12 days and 10 days on Cry5B-producing JM103. Lifespan of *ifo-1(kc3)* on control bacteria was also reduced compared with N2 (14 days, $n=39$ versus 16 days, $n=117$, $P<0.05$) and Cry5B intoxication resulted in decreased survival that was similar to the wild type (12 days, $n=38$ versus 12 days, $n=111$, $P>0.05$).

Taken together, the effects of Cry5B on larval arrest, time of larval development and, to some degree, also on lifespan were enhanced in the *n678* and *kc2* backgrounds, with the strongest effects in *kc2*, i.e. in a situation in which the endotube was most severely affected before Cry5B treatment.

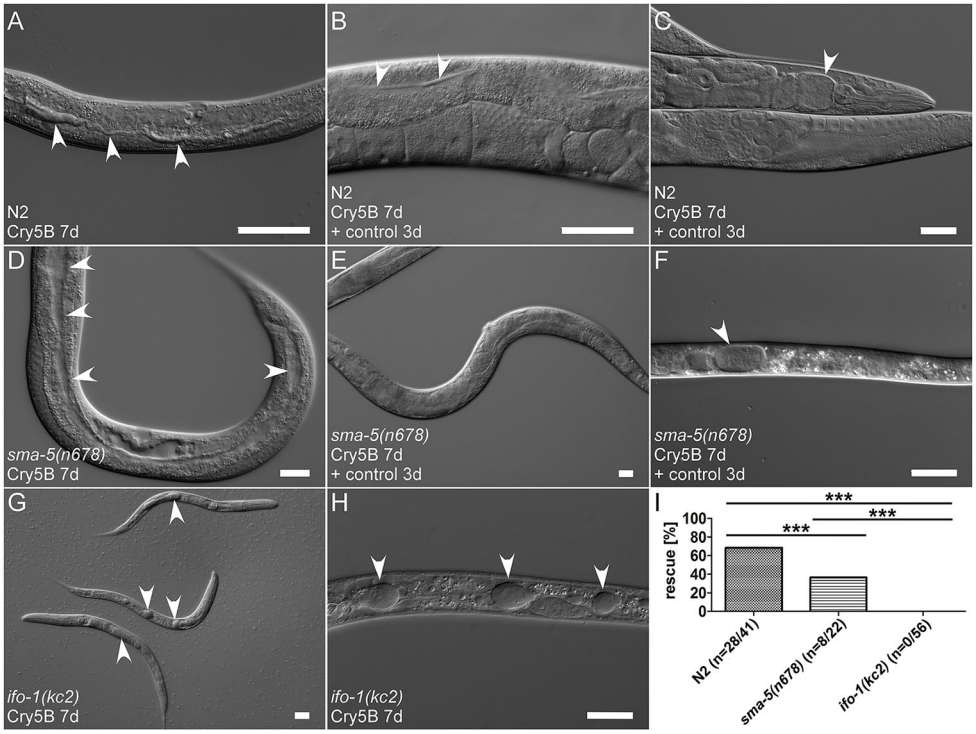

Fig. 4. The Cry5B intoxication phenotype can be partially rescued depending on the severity of the pre-existing endotube damage. (A-H) Interference contrast images and (I) quantification of Cry5B intoxication phenotype rescue under different conditions. (A) The wild-type animal was grown on Cry5B-producing JM103 bacteria and arrested at L3 stage, exhibiting multiple luminal dilations (arrowheads). Transfer of arrested larvae to control JM103 allowed 68.29% ($n=28/41$) to reach adulthood (I). Some rescued animals display a normal intestinal lumen (B, arrowheads), whereas others do not (C, arrowhead). (D-F) Most *sma-5(n678)* animals arrest as larvae on Cry5B-producing bacteria, presenting luminal dilation (arrowheads in D). Only 36.36% ($n=8/22$) of these animals can be rescued by transferring them to control bacteria (E,I), whereas 63.64% ($n=14/22$, $P<0.001$) die as larvae with huge luminal dilations (F, arrowhead). (G,H) In the case of *ifo-1(kc2)*, 100% of Cry5B-intoxicated larvae arrest with huge luminal dilations (arrowheads in G,H) and cannot be rescued by transfer to control bacteria ($n=0/56$, $P<0.0001$; I). The rescue rate (%) was calculated by determining the ratio of adult animals and the total number of viable larvae after 7 days of Cry5B treatment. ***$P<0.001$. Scale bars: 50 µm in A-C; 20 µm in D-H.

Development (2019) 146, dev169482. doi:10.1242/dev.169482

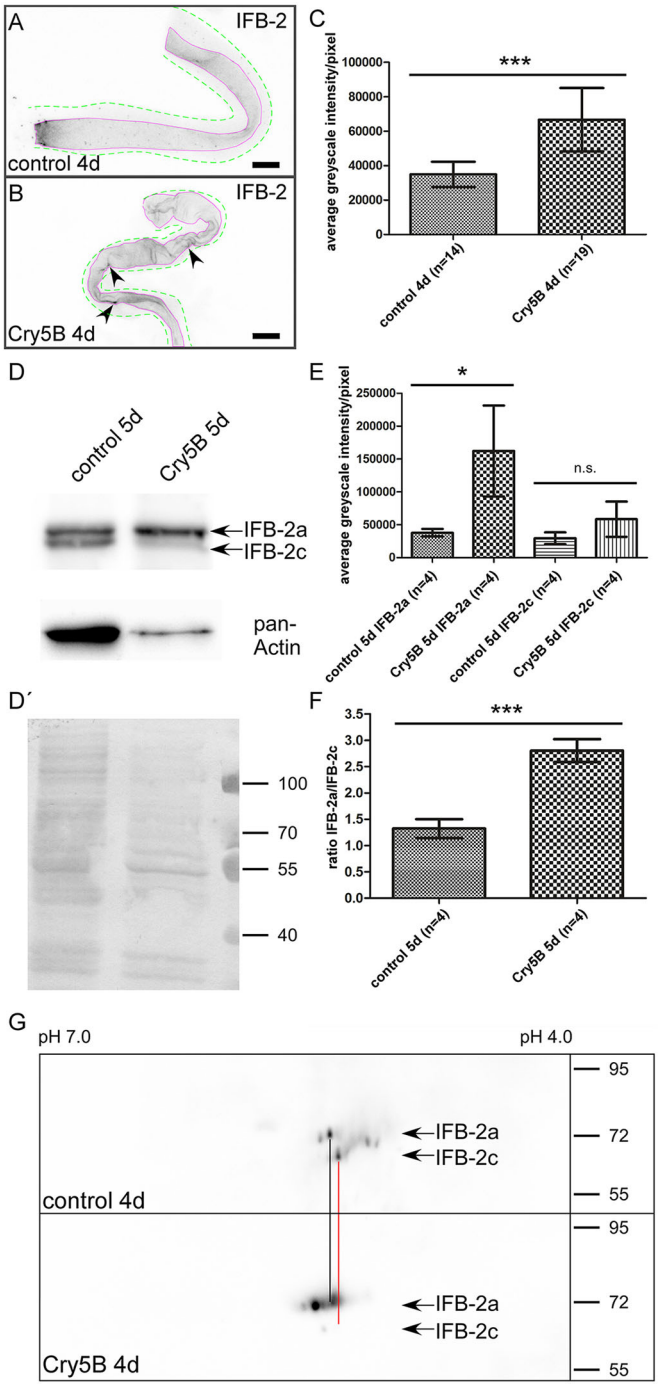

Fig. 5. Cry5B intoxication induces IFB-2 overexpression, a shift of IFB-2 isoform expression and altered IFB-2 phosphorylation. (A-B) Representative immunofluorescence images detecting IFB-2 in isolated intestines extracted from N2 that were grown for 4 days (4d) either on control (A) or on Cry5B-producing JM103 bacteria (B). Whereas the control intestine displays a uniform distribution of IFB-2, the Cry5B-treated intestine shows local accumulations (arrowheads). Regions used for quantification are outlined in purple; outline of intestinal cells is marked by green dotted line. Scale bars: 20 µm. (C) Quantification of immunofluorescence reveals an increased expression of IFB-2 after Cry5B treatment (66,730±18,400 average greyscale intensity/pixel, n=19) compared with the control (34,974±7359 average greyscale intensity/pixel, n=14; P<0.0001). (D) Representative immunoblot analysis detecting IFB-2 isoforms a and c (upper panel) and pan-actin (lower panel) in lysates that were obtained from worms grown for 5 days (5d) on control (left lane) or Cry5B-producing JM103 (right lane). D′ shows corresponding Ponceau S staining as an additional loading control, with positions of co-electrophoresed molecular weight markers in kDa in the right margin. Note the overall increased expression of IFB-2 with a concurrent shift towards the longer isoform upon Cry5B treatment. (E,F) Quantitative analyses of anti-IFB-2 immunoblots of N2 lysates after 5 days on control or Cry5B-producing JM103 (n=4; mean±s.d.). Average greyscale intensity/pixel measured for the IFB-2a and IFB-2c immunosignals (control IFB-2a: 37,851 ±5700 versus Cry5B IFB-2a: 162,161±69,182, P=0.0116; control IFB-2c: 29,511±8937 versus Cry5B IFB-2c: 58,463±26,812. P>0.05.) (E). Immunoblot quantification of the IFB-2a/IFB-2c ratios (2.80±0.21 versus 1.32±0.18; P<0.0001) (F). (G) Immunoblots of total N2 worm lysates separated by two dimensional polyacrylamide gel electrophoresis and reacted with anti-IFB-2 antibodies. The worms were grown on control (top) or on Cry5B-producing bacteria for 4 days. Note the Cry5B-induced shifts towards the larger isoform and of both IFB-2 isoforms to more basic isoelectric variants indicating reduced IFB-2 phosphorylation. Position of co-electrophoresed molecular weight markers is shown in kDa on the right. Data are mean±s.d.; *P=0.0116, ***P<0.0001. n.s., not significant.

Cry5B-induced developmental arrest can be reversed depending on the severity of the pre-existing endotube impairment

Next, we wanted to find out whether and in which way the presence of the endotube affects repair mechanisms after Cry5B intoxication. To this end, arrested larvae that had survived 7 days of Cry5B treatment (examples in Fig. 4A,D,G,H) were placed on control JM103 for 3 days (Fig. 4B,C,E,F). This resulted in reversal of larval arrest in 68.29% of N2. It was accompanied by reversal of intestinal alterations in some but not all animals (Fig. 4B,C,I). Remarkably, 36.36% of *sma-5(n678)* worms also reached adulthood upon Cry5B removal (Fig. 4E,I). Yet, the majority died with pronounced intestinal pathologies (Fig. 4F). No rescue was observed for *ifo-2(kc2)* (Fig. 4I).

Cry5B intoxication enhances expression of the intermediate filament protein IFB-2 and induces a switch in IFB-2 isoform expression

We then wanted to examine how microbial and toxin stress affects the intestinal IFs, as they are the major endotube components. Transcriptome analyses had already shown that *ifd-2* mRNA is upregulated (see above). To find out whether the expression of other intestinal IFs is affected and to see whether IF protein expression is altered, we focused on IFB-2, as suitable reagents were available (Francis and Waterston, 1991; Hüsken et al., 2008). First, fluorescence intensity was determined in dissected immunostained intestines from N2 that were grown either on control JM103 or on Cry5B-producing JM103 bacteria for 4 days. In contrast to the uniform distribution of IFB-2 in control intestines, local accumulations and cytoplasmic invaginations were observed upon Cry5B intoxication (Fig. 5A,B). Furthermore, quantification on sum-slice projections revealed an increased expression of IFB-2 after Cry5B treatment compared with control intestines (Fig. 5C). To validate this change in IFB-2 expression, immunoblots were carried out on whole-worm lysates. Quantification not only showed that overall IFB-2 expression was increased after Cry5B treatment but also revealed a shift in isoform expression resulting in a significant increase of the IFB-2a/IFB-2c ratio (Fig. 5D-F). In addition, a shift to hypophosphorylated IFB-2 isoforms was detected by two-dimensional gel electrophoresis and immunoblotting (Fig. 5G).

IFB-2 knockout prevents endotube formation and leads to increased Cry5B sensitivity

To find out whether and to what degree IFs contribute to the increased Cry5B sensitivity of *ifo-1* and *sma-5* mutants, we generated an *ifb-2* knockout. The mutant *ifb-2* allele *kc14* contains a thymidine insertion at position 41 of the *ifb-2* open

Development (2019) 146, dev169482. doi:10.1242/dev.169482

reading frame leading to a premature stop in the second exon, which allows translation of 29 amino acids, including only the first 13 aminoterminal amino acids of IFB-2 (Fig. S4A). Immunoblot analyses showed the complete absence of the IFB-2 signal, which confirmed that *kc14* is a full knockout allele (Fig. S4B). Electron microscopy further revealed the complete absence of the electron-dense endotube (Fig. 6A,B). This was surprising in light of the presence of several other intestinal IF proteins. But a recent publication provided evidence that IFB-2 heteropolymerizes with most, if not all, other IF polypeptides (Karabinos et al., 2017). Surprisingly, microvilli still appeared to be mostly intact. Microvillar actin bundles emanated into the apical cytoplasm with characteristic actin rootlets (Fig. 6B). In addition, the *C. elegans* apical junction appeared to be normal except for a lack of associated IFs and multiple microtubules in close vicinity (Fig. S5).

Next, we tested the response of *ifb-2(kc14)* worms to Cry5B intoxication. Larval arrest was virtually absent on control JM103 (0.67%) but was almost complete and considerably higher than in N2 controls on Cry5B-synthesizing JM103 (Fig. 6C). Similarly, whereas the time of larval development was slightly increased in *kc14* mutants compared with the wild type (0.2 days), it was more increased in Cry5B-intoxicated *kc14* mutant worms compared with the wild type (1.8 days; Fig. 6D). Furthermore, *ifb-2(kc14)* progeny was considerably reduced on control JM103 in comparison with wild-type N2 (155±24, n=24 versus 271±25, n=24; P<0.0001). Surprisingly, the lifespan of *ifb-2(kc14)* on control JM103 was increased compared with the wild type. However, this was considerably reduced on Cry5B-producing JM103 (Fig. 6E).

Endotube dysfunction correlates with impaired oxidative and osmotic stress resistance

It has been suggested that microbial infections induce oxidative stress in *C. elegans* (Bolm et al., 2004; Miller et al., 2015; Sem and Rhen, 2012). We therefore treated worms with paraquat that is commonly used as an oxidative stress inducer (Senchuk et al., 2017). Fig. 7A shows that dead animals are detected much earlier in all endotube mutants than in N2, revealing increasing lethality from N2 to *ifb-2(kc14)*, to *sma-5(n678)* and *ifo-1(kc2)*.

To explore whether the increased sensitivity of the endotube mutants to microbial, toxin and oxidative stresses reflects an overall increased vulnerability, we tested their osmotic stress resistance. Osmotic stress resistance is considered to be one of the most important properties of a functional epithelial barrier and has been linked to IFs (D'Alessandro et al., 2002; Pekny and Lane, 2007). To

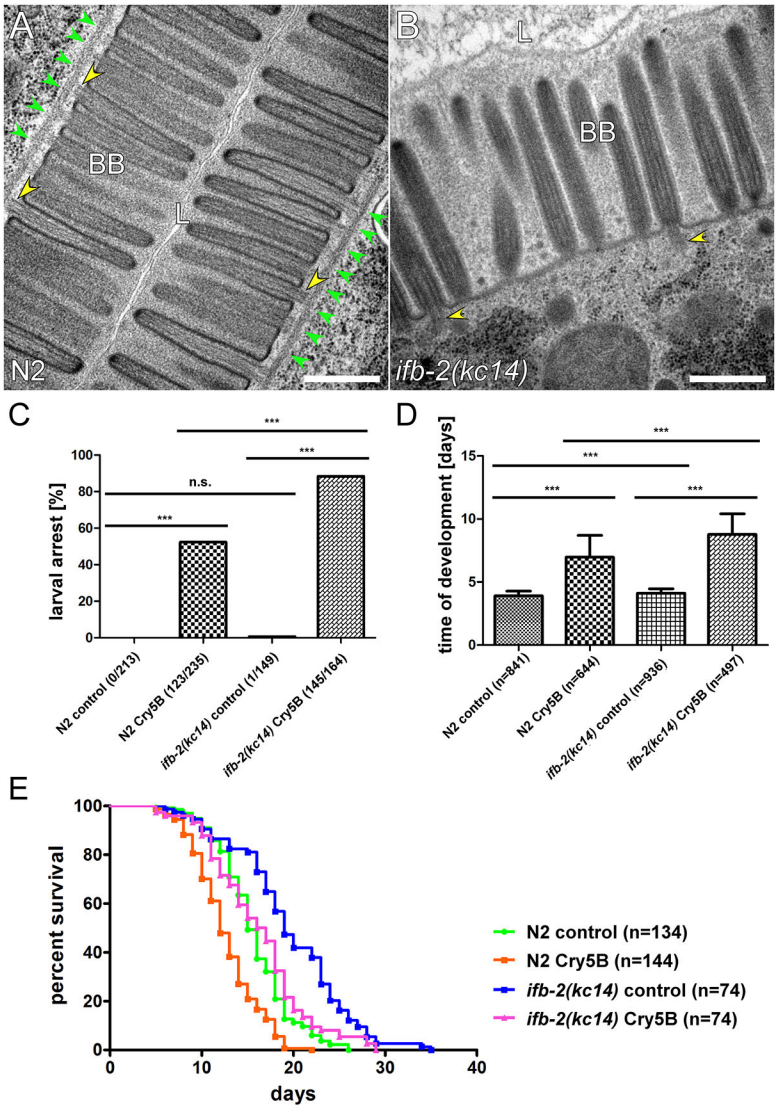

Fig. 6. Knockout of the intestinal IF protein IFB-2 prevents endotube formation and leads to increased Cry5B sensitivity. (A,B) Electron micrographs of young adult N2 (A) and *ifb-2(kc14)* knockout animals (B). (A) Wild-type worms show properly arranged microvilli, which are anchored through actin filament bundles (yellow arrowheads) to the electron-dense endotube (green arrowheads). (B) IFB-2 depletion results in complete loss of the electron-dense endotube. Note that microvillar actin bundles still extend into the apical cytoplasm (yellow arrowheads). BB, brush border; L, intestinal lumen. Scale bar: 500 nm. (C) Only 0.67% (1/149) larval arrest is observed in *ifb-2(kc14)* mutants grown on control JM103 (no larval arrest in N2; 0/213; P>0.05) and 88.41% (145/164; P<0.0001) larval arrest is observed in *ifb-2(kc14)* grown on Cry5B-producing JM103 versus 52.34% (123/235, P<0.0001) for wild-type N2. (D) Cry5B intoxication prolongs time of development in *ifb-2(kc14)* (control JM103: 4.12±0.35 days, n=936 versus Cry5B-producing JM103: 8.77±1.64 days, n=497; P<0.0001) even more than in the wild type [3.91±0.37 days (n=841) on control versus 6.97±1.72 days (n=644) on Cry5B; P<0.0001]. Note also that *ifb-2(kc14)* animals grown on control JM103 show a slightly increased time of larval development compared with N2 (P<0.0001). (E) Lifespan analysis (plot of the Kaplan–Meier estimator) shows that *ifb-2(kc14)* animals survive longer than the wild type in control conditions [19 days for *ifb-2(kc14)* (n=74) and 15 days for N2 (n=134, P<0.0001]. *ifb-2(kc14)* shows severe reduction of lifespan on Cry5B-producing bacteria, which, however, is still longer than in the wild-type control [*ifb-2(kc14)*: 16.5 days, n=74; N2: 12 days, n=144; P=0.0004]. Larval arrest rates (%) were calculated from the ratios of animals dying as larvae and as adult. Data are mean±s.d.; ***P<0.0001. n.s., not significant.

Development (2019) 146, dev169482. doi:10.1242/dev.169482

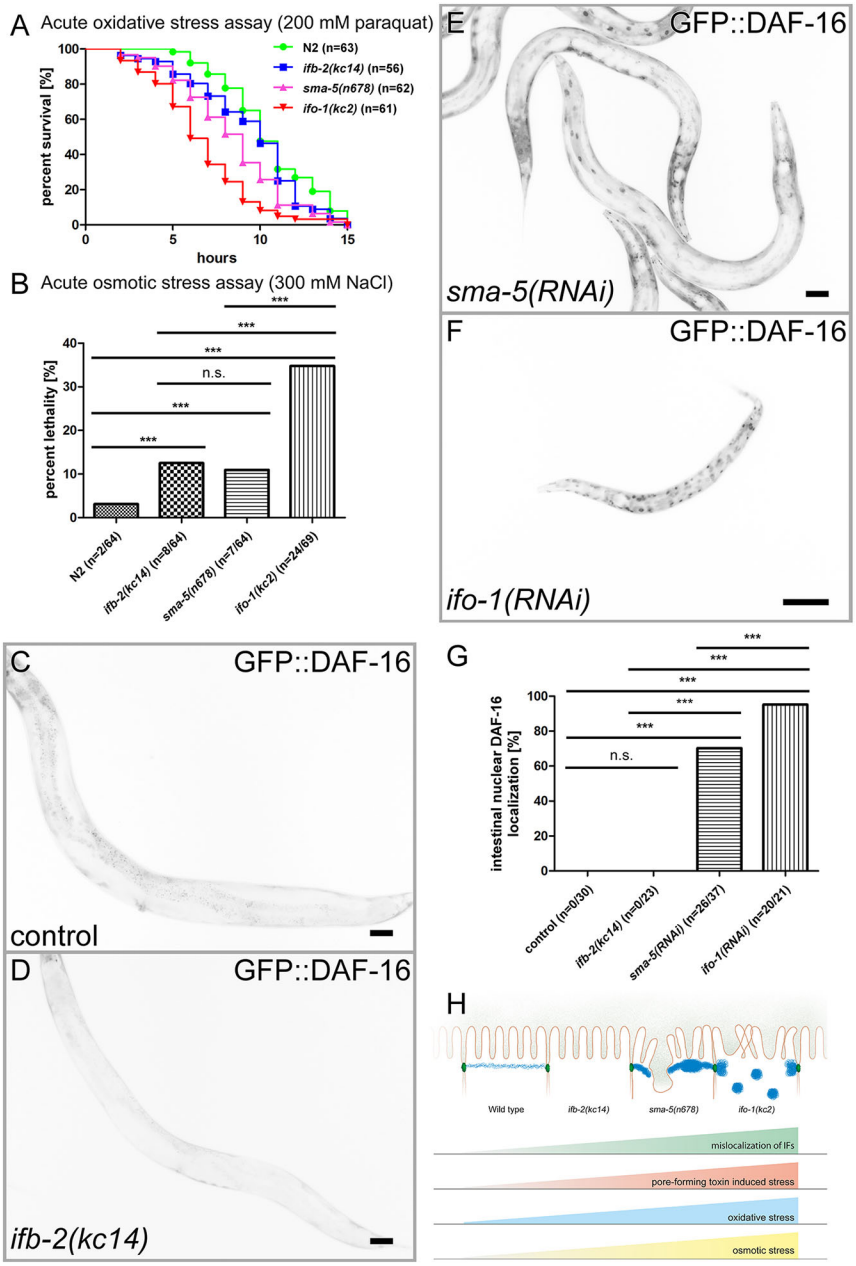

Fig. 7. Endotube perturbation leads to increased sensitivity towards different stress conditions. (A) Wild-type and *ifb-2(kc14)* animals show similar median survival when exposed to 200 mM paraquat (10 h; *n*=63 and *n*=56, respectively). However, *ifb-2(kc14)* show a tendency to die a bit earlier. Notably, mutants with pronounced endotube re-localization show significant reduction of survival depending on the severity of IF mislocalization [*sma-5(n678)*: 9 h, *n*=62, *P*<0.001; *ifo-1(kc2)*: 6 h, *n*=61, *P*<0.0001]. Survival data are represented as a plot of the Kaplan–Meier estimator. (B) The wild type tolerates 300 mM sodium chloride-induced osmotic stress, with a very low lethality rate (3.125%, *n*=2/64), whereas mutants with impaired endotube show increased lethality depending on the severity of IF mislocalization [*ifb-2(kc14)*: 12.50%, *n*=8/64, *P*<0.0001; *sma-5(n678)*: 10.938%, *n*=7/64, *P*<0.001; *ifo-1(kc2)*: 34.783%, *n*=24/69, *P*<0.0001]. Survival rates (%) were calculated from the ratios of animals either dying or surviving after a chase period of 24 h. (C-F) The fluorescence micrographs depict increased GFP::DAF-16 localization in the intestinal nuclei of *sma-5(RNAi)*- and *ifo-1(RNAi)*-treated animals even in the absence of stress inducers (E,F), whereas the GFP::DAF-16 distribution in the *ifb-2(kc14)* background is indistinguishable from the wild-type control treated with control RNAi (C,D). (G) Quantification of nuclear GFP::DAF-16 localization in the different genetic backgrounds [control: 0%, *n*=0/30; *ifb-2(kc14)*: 0%, *n*=0/23; *sma-5(RNAi)*: 70.27%, *n*=26/37; *ifo-1(RNAi)*: 95.24%, *n*=20/21; control versus *ifb-2(kc14)*, *P*>0.05; control versus *sma-5(RNAi)*, *P*<0.0001; control versus *ifo-1(RNAi)*, *P*<0.0001; *ifb-2(kc14)* versus *sma-5(RNAi)*, *P*<0.0001; *ifb-2(kc14)* versus *ifo-1(RNAi)*, *P*<0.0001]. (H) Scheme to summarize the major observations of the manuscript, highlighting the increasing stress sensitivity of mutants lacking an endotube to the most severe endotube alterations observed in *ifo-1(kc2)*. Data are mean±s.d. ***P*<0.0001. n.s., not significant.

this end, worms were first exposed to 300 mM sodium chloride for 24 h. After a chase period of another 24 h 62/64 wild-type N2 survived. In contrast, 56/64 *ifb-2(kc14)*, 57/64 of *sma-5(n678)* and only 45/69 *ifo-1(kc2)* survived (Fig. 7B). Remarkably, even in the absence of stress, loss of either SMA-5 or IFO-1 leads to nuclear DAF-16 localization in the intestine [*sma-5(RNAi)*: 70.27%; *ifo-1(RNAi)*: 95.24%] whereas loss of IFB-2 does not [*ifb-2(kc14)*: 0%] (Fig. 7C-G).

DISCUSSION

Using the genetic model organism *C. elegans*, we examined whether and how the IF-rich intestinal endotube, which is positioned at the junction between the organelle-free terminal web and the apical cytoplasm, responds to microbial infection and intoxication. By infecting worms with *B. thuringiensis* or treating them with the pore-forming toxin Cry5B, we found drastic alterations of the endotube, manifesting initially as local thickening, followed by thinning and disruption at later stages, all of which was accompanied by luminal widening and formation of cytoplasmic invaginations. These observations are reminiscent of reports on worms that were infected with the microsporidian parasite *Nematocida parisii* (Estes et al., 2011; Troemel et al., 2008). In this case, however, the parasite induced rearrangement of the apical actin and IF cytoskeleton to support non-lytic exit of the intracellularly produced spores. Intestinal alterations with endotube re-organization have also been observed in naturally occurring, virally infected *Caenorhabditis* isolates (Félix et al., 2011). Our findings are compatible with the consequences of treating worms with the fungal *Coprinopsis cinerea* lectin 2 (CCL2), which is a non-immunoglobulin carbohydrate protein (Stutz et al., 2015). These animals presented brush border defects and enlarged intestinal lumina with endotube gaps and multiple small apical

Development (2019) 146, dev169482. doi:10.1242/dev.169482

plasma membrane invaginations. Interestingly, localized endotube heterogeneities were also reported for mutants of *act-5*, which is the major microvillar actin isoform (MacQueen et al., 2005). In this example, shortening and absence of microvilli is associated with endotube thickening. This may be interpreted as a compensatory mechanism much like the initial endotube thickening that is observed during Cry5B intoxication.

The results of our study go beyond previous reports by demonstrating that the major endotube component IFB-2 is not merely a bystander of apical cell rearrangement upon microbial insult but responds actively through increased IFB-2 levels and a switch in IFB-2 isoform expression. Of note, we observed a similar switch in IFB-2 isoform expression in *ifo-1(kc2)* animals (Geisler, 2014). Increased IFB-2 synthesis was also recently detected in a proteomic study that compared *C. elegans* infected with either pathogenic or non-pathogenic *B. thuringiensis* strains (Treitz et al., 2015). Interestingly, IFC-2 and IFD-2 were also upregulated in this study, which is further supported by our finding of increased *ifd-2* mRNA synthesis in Cry5B-treated worms. We propose that the increased synthesis of intestinal IF proteins is responsible for endotube thickening as a last line of defense against the microbial stressors. Whether the switch in isoform expression confers specific properties onto the IF cytoskeleton remains to be shown. The importance of IF protein expression levels and isotype production for stress protection has also been emphasized in the murine intestine, as was reported in a recent publication (Asghar et al., 2015). In case of the nuclear lamin IFs, abundant evidence has been accumulated that expression levels are one of the major factors that determine mechanical cell properties in many different organ systems and species (Cho et al., 2017; Swift et al., 2013).

We propose that the endotube acts as a protective intracellular barrier against microbe-induced pathogenesis. This may be accomplished by providing a mechanical fence, which seals and separates the apical cytoplasm from the rest of the cell, or by providing an adsorptive surface to immobilize potentially harmful proteins and other substances. Using well-defined endotube mutants we were able to demonstrate that endotube alterations lead to increased Cry5B toxicity that results in enhanced larval arrest, increased time of development and reduced lifespan. Of note, similar effects were also elicited with other *B. thuringiensis* toxins (i.e. Cry21EaI, Cry21FaI and Cry21GaI; data not shown). Complete endotube loss in *ifo-1(kc2)* was associated with enhanced alterations compared with partial endotube loss in *sma-5(n678)*. We were further able to link this protective endotube function to IFB-2, the absence of which led to enhanced larval arrest and increased time of development. Comparable developmental arrest has been reported in starved animals (Baugh, 2013; Kaplan et al., 2015). Given that the *sma-5(n678)* and *ifo-1(kc2)* mutants are small, compromised nutrient uptake may also contribute to the toxin effects on larval development that is observed in our current study. We could further show that endotube function includes protection against oxidative and osmotic stress, indicating that it serves an overall stress-protective role. The differences in stress resilience of the different mutant backgrounds remain to be fully untangled. Obviously, complete absence of an endotube in *ifb-2(kc14)* is better tolerated than a partially disrupted endotube in *sma-5(n678)* or an endotube that is collapsed onto the *C. elegans* apical junction in *ifo-1(kc2)* (Fig. 7H). It is possible that the altered endotube elicits a dominant negative effect on intestinal function, e.g. by interfering with junctional signaling or vesicle trafficking. The relevance of our findings for distant species is suggested by the reported development of colitis and reduced stress resilience in the intestine of mice and humans with mutated keratins (Asghar et al., 2015; Habtezion et al., 2005; Helenius et al., 2016; Owens and Lane, 2003; Zupancic et al., 2014). Moreover, the barrier function of epithelial IF proteins is not restricted to the intestine but appears to be relevant also in the placenta (Jaquemar et al., 2003) and even in skin development (Kumar et al., 2015).

Complex results were obtained in lifespan analyses. As expected, the lifespan of *ifo-1(kc2)* was reduced in comparison with N2. Contrary to our previous observations, however, *sma-5(n678)* did not show a reduced lifespan. This may be because of the use of JM103 as feeding bacteria in the current study instead of OP50, which had been used in former work and is known to be a mild pathogen in *C. elegans* (Darby, 2005). Surprising was the increased lifespan of *ifb-2(kc14)*, which may be caused by activation of pathways in response to endotube loss. This notion is supported by the rather minor microvillar perturbation in *ifb-2(kc14)* in comparison with the major brush border disturbances observed in *sma-5(kc678)* and *ifo-1(kc2)* mutants (Carberry et al., 2012; Geisler et al., 2016).

An interesting link between pore-forming toxins and endotube organization has been provided by Kao et al. (2011). They identified IFO-1 as a target of Cry5B pore-forming toxin-regulated MAPK. The redistribution of IFO-1 that is reported in our current paper and its known role in intestinal filament organization provides a link to a function in Cry5B protection. Furthermore, the pore-forming toxin-induced MAPK SEK-1, which is involved in p38 signaling and the JNK-family MAPK KGB-1 (Huffman et al., 2004), may affect IF phosphorylation, which has been linked to altered endotube structure in *sma-5* mutants (Geisler et al., 2016). In addition, the observed sequestration of SMA-5 to cytoplasmic dots, which possibly correspond to vesicular structures, may result in a loss of SMA-5 function and thereby further enhance IF reorganization and endotube disorganization through altered phosphorylation. A possible link between IFO-1 and SMA-5 is also provided by our observation that SMA-5 accumulates in cytoplasmic dots in *ifo-1(RNAi)* animals.

Our findings on the increased expression of innate immune response genes in Cry5B-intoxicated animals extend previous reports (Huffman et al., 2004; Kao et al., 2011). We find it particularly interesting that innate immune response genes are already switched on in *ifo-1(kc2)* in the absence of specific pathogen. This may be explained by the reported mild pathogenicity of the OP50 *E. coli* feeding strain that is routinely used in *C. elegans* laboratories (Alper et al., 2007). Our findings are paralleled by observations in cultured human intestinal cells and murine intestine revealing links between cytokine and keratin expression, with consequences for barrier formation (Wang et al., 2007). Furthermore, evidence is also accumulating for a crosstalk between keratins and innate immunity in multiple epithelial cell types (Habtezion et al., 2005; Lessard et al., 2013; Lu et al., 2007; Roth et al., 2012; Salas et al., 2016). Using *C. elegans* will help to further untangle the different molecular mechanisms that link cytoskeletal network organization to microbe-induced response reactions.

MATERIALS AND METHODS

DNA constructs

To prepare CRISPR *ifb-2* knockout construct #4113 rolling circle mutagenesis PCR was performed using the Q5® Site-Directed Mutagenesis Kit (New England Biolabs). Empty sgRNA cassette of plasmid pDD162 (*Peft-3::cas9*+empty sgRNA, Addgene plasmid #47549, deposited by Bob Goldstein) was mutated by inserting *ifb-2*-encoding

Development (2019) 146, dev169482. doi:10.1242/dev.169482

sgRNA using primers 16-004 (TGATGAGGAGGATGTAGTTGGTTTTAG-AGCTAGAAATAGCAAGT) and 15-010 (CAAGACATCTCGCAATAGG).

To enable in-frame insertion of a YFP-encoding cassette into the *ifc-2a* gene, CRISPR *ifc-2a* targeting plasmid #4110 and repair template plasmid #4102 were constructed. For preparing plasmid #4110, rolling circle mutagenesis PCR was performed with the help of the Q5® Site-Directed Mutagenesis Kit on plasmid pDD162 using primers 15-015 (ATTTGAA-GAGGAGTAGGAGGTTTTAGAGCTAGAAATAGCAAGT) and 15-010. For the repair template, two homology arms covering the 3′-end of the *ifc-2a* open reading frame were PCR-amplified from purified genomic wild-type DNA using primer pairs 15-136/15-137 (ATACGC**AAGCTT**-TCACAAGTTCTGCGCCTCAC and CGCATA**ACCGGT**GATTTGAA-GAGGAGTAGGAGTGATGGCTCTGTTG, respectively) and 15-138/15-139 (ATACGC**ACCGGT**AAGGATGCTCTTTCTTAATG and ATACGC-**GGATCC**CTGGGGTCTGACTTCAATGC, respectively). The resulting fragments were cut with *Hin*dIII/*Age*I and *Age*I/*Bam*HI, respectively, and cloned together into the *Hin*dIII/*Bam*HI sites of plasmid pUC18 (Addgene plasmid #50004, deposited by Joachim Messing) thereby generating plasmid #4100. Subsequently, the eYFP-encoding sequence of plasmid Krt8::YFP (Schwarz et al., 2015) was PCR-amplified with primers 15-140/15-141 (ATACGC**ACCGGT**CCATGGTGAGCAAGGGCGAG and ATACGC**ACCGGT**TTACTTGTACAGCTCGTC, respectively), digested with *Age*I, and inserted into the *Age*I site of plasmid #4100, resulting in the repair template plasmid #4102. Bold letters mark the restriction sites used for cloning.

C. elegans strains and bacteria

Wild-type Bristol strain N2 and strain FK312 *sma-5(n678)X* were obtained from the *Caenorhabditis* Genetics Center (CGC; University of Minnesota, USA). Strain CF1934 *daf-16(mu86)I;muIs109[daf-16p::gfp::daf-16+odr-1p::rfp]* was kindly provided by Malene Hansen (Sanford Burnham Prebys Medical Discovery Institute, CA, USA; Kumsta and Hansen, 2012). Strains BJ49 *kcIs6[ifb-2p::ifb-2a::cfp]IV* (Hüsken et al., 2008), BJ186 *kcIs30[ifo-1p::ifo-1::yfp;myo-3p::mCherry::unc-54]III* (Carberry et al., 2012), BJ263 *kcEx73[WRM0633B_G09(pRedFlp-Hgr)(sma-5[26688]::S0001_pR6K_Amp_2xTY1ce_EGFP_FRT_rpsl_neo_FRT_3xFlag)dFRT::unc-119-Nat];unc-119 (ed3)III* (Geisler et al., 2016), BJ142 *ifo-1(kc2)IV* and BJ143 *ifo-1(kc3)IV* (Carberry et al., 2012) have been recently described.

ifb-2(kc14) knockout strains were obtained by microinjection of plasmids #4113 and pCFJ104 [*myo-3p::mCherry::unc-54*] (kindly provided by Christian Frøkjær-Jensen, University of Utah, USA; Frøkjær-Jensen et al., 2008) into gonads of young adult animals of strain BJ49. F1 progeny was screened for animals expressing the co-injection marker. The F2 generation was then screened for IFB-2a::CFP-negative animals. Full knockout was confirmed using immunohistochemistry and immunoblotting. Worms were outcrossed four times with wild-type N2. The resulting strain BJ309 was used in this study. Strain CF1934 was crossed with BJ309 giving rise to strain BJ342 *ifb-2(kc14);daf-16(mu86)I;muIs109[daf-16p::gfp::daf-16 +odr-1p::rfp]*.

In order to create an *ifc-2(kc16)* knock-in strain, a mixture containing 10 ng/µl repair template plasmid #4102, 50 ng/µl *ifc-2a* targeting plasmid #4110 and 50 ng/µl co-injection marker plasmid pCFJ104 was injected into the distal gonad arms of young adult wild-type animals. The F1 generation was screened for transgenic animals that expressed the co-injection marker, and F2 progeny was further screened for YFP-positive animals. After loss of the extrachromosomal array, the insertion of the fluorescence tag was verified by PCR analysis and the homozygous strain was outcrossed six times with wild-type N2, resulting in strain BJ316.

OP50 bacteria were obtained from the CGC. JM103 *E. coli* carrying either the pQE9 control vector (referred to as control JM103) or the pQE9 vector containing the Cry5B gene (referred to as Cry5B-producing JM103) were kindly provided by Raffi Aroian (UMASS Medical School, MA, USA; Bischof et al., 2006). *B. thuringiensis* strain DB27 was kindly shared by Ralf J. Sommer (Max Planck Institute for Developmental Biology, Germany; Rae et al., 2010). RNAi by feeding was performed as previously described (Geisler et al., 2016) without supplement of tetracycline.

Intoxication and infection assays

For Cry5B intoxication experiments, control JM103 or Cry5B-producing JM103 were grown overnight in Luria broth (LB) with 100 µg/ml ampicillin and 7 µl/ml 1 M isopropyl β-d-1-thiogalactopyranoside (IPTG) and 300 µl aliquots were placed on nematode growth medium (NGM) plates containing 100 µg/ml ampicillin and 2 mM IPTG. For *B. thuringiensis* assays, liquid overnight cultures of OP50 and DB27 were prepared in LB without additives and 300 µl aliquots were put on NGM plates without additives. The inoculated plates were incubated overnight at room temperature and plates were stored at 4°C for up to two weeks without detectable loss of bacterial and toxin activity. Intoxication and infection experiments were started by transferring adult worms into 70 µl bleaching solution containing 1 ml PBS, 150 µl 13% NaOCl and 100 µl 4 M NaOH next to the bacterial lawn. Mother animals dissolved, releasing embryos that survived owing to their crude eggshell. Plates were incubated at 18°C during the entire experimental period and animals were transferred at least every 3 days onto new plates.

Propidium iodide staining

Wild-type L4 larvae were placed for 24 h at 20°C on Cry5B-containing JM103 and corresponding control plates. Subsequently, a propidium iodide solution (6.7 µl/ml dissolved in dH_2O; Sigma-Aldrich) was pipetted on the bacterial lawn and then the plates were incubated for 2 h. Animals were then mounted on agar pads for imaging.

Stress assays

Methyl viologen dichloride hydrate (paraquat; Sigma-Aldrich) was used for oxidative stress assays at a final concentration of 200 mM in NGM agar (Senchuk et al., 2017). Poured plates were stored overnight at room temperature following inoculation with 50 µl 10× concentrated overnight culture of OP50. After additional incubation for 2 days at room temperature, plates were ready to use or could be stored for up to 3 days at 4°C before use. L4 larvae were transferred onto the bacterial lawn and incubated at 18°C. Individual worms were scored each hour for viability using mechanical stimulation with a platinum wire. Animals with no response were scored as dead. Statistical analysis was performed using the survival function and the Gehan–Breslow–Wilcoxon Test of GraphPad Prism 5.01.

For osmotic stress assays, NGM agar containing 300 mM NaCl was used. Normal NGM plates with 50 mM NaCl were used as controls. Poured plates were incubated overnight at room temperature followed by inoculation with 50 µl overnight culture of OP50 and another overnight incubation at room temperature. L4 larvae were transferred to the bacterial lawn of each plate and incubated for 24 h at 18°C. Individual worms were then washed in recovery buffer (M9 buffer with 150 mM NaCl) and subsequently transferred to the bacterial lawn of a normal NGM plate. After another 24 h at 18°C the viability of each animal was tested as described above. Significance was calculated using the chi-square function of Excel (Microsoft).

For the DAF-16 stress assay of IFO-1- and SMA-5-depleted worms, L4 larvae of strain CF1934 were treated with *ifo-1(RNAi)* and *sma-5(RNAi)* for 2 days at 18°C by feeding. The animals were then placed on new RNAi plates for 5 days at 18°C before imaging of the resulting progeny. For DAF-16 stress assay of IFB-2-depleted worms, adult CF1934 and BJ342 worms were first placed into 70 µl bleaching solution next to the bacterial lawn of empty vector-containing HT115 feeding bacteria and incubated for 5 days at 18°C. Animals were then mounted on agar pads for imaging.

Transcriptome analysis

Transcriptome analyses were performed on dissected intestines of wild-type and *ifo-1(kc2)*-mutant worms that were grown on OP50 bacteria. To this end, L4 larvae were suspended in ddH_2O containing 1% (w/v) levamisole (Sigma-Aldrich), incised either at their anterior or posterior end to extrude intestines. Intestines were cut off, collected with a capillary and transferred directly into an excess of RNA extraction buffer (Arcturus PicoPure RNA Isolation Kit, Thermo Fisher Scientific). For each wild-type pool, 40 intestines were collected, and 80 were collected for each pool of the smaller *ifo-1(kc2)* mutants, before processing them according to the protocol

Development (2019) 146, dev169482. doi:10.1242/dev.169482

provided by the manufacturer. The purification included an on-column DNAse digest using the peqGOLD DNase I Digest Kit (Peqlab). For gene chip analysis, three independent RNA isolates were used.

To assess transcriptional effects of Cry5B intoxication, mRNA levels were analyzed after growing wild-type worms either on control JM103 or Cry5B-producing JM103 bacteria. This was done by transferring adult wild-type animals into 70 µl of bleaching solution, which was pipetted next to the bacterial lawn of the culture plate. Plates were incubated for 4 days at 18°C when worms had reached L4 or young adult stage. Worms were then washed three times in ice-cold M9 medium to remove remaining bacteria. Pelleted worms were ground thoroughly with mortar and pestle under liquid nitrogen. A maximum of 100 mg tissue powder was then transferred into an RNase-free, liquid nitrogen-cooled, 2 ml microcentrifuge tube and the following steps were performed according to the RNeasy Plant Mini Kit (Qiagen) including an on-column DNAse digest using the peqGOLD DNase I Digest Kit. For gene chip analysis three independent RNA isolates were used.

The quality of the isolated total RNA was assessed by determining the RNA integrity number (RIN factor) with the help of an Agilent 2100 bioanalyzer (Agilent Technologies). GeneChip WT cDNA Synthesis and Amplification, GeneChip WT Terminal Labeling and GeneChip Sample Cleanup Module kits (all from Affymetrix) were used to prepare labelled cDNA for hybridization with the GeneChip *C. elegans* 1.0 ST Array from Applied Biosystems using a GeneChip Fluidics Station 450 (Affymetrix). Hybridization signals were quantified with a GeneChip Scanner 3000 7G and analyzed with the help of Affymetrix Expression Console software. Tissue specific gene expression was analyzed by entering the WormBase IDs into WormExp (Yang et al., 2016). The following categories were scored as intestinal using standard settings: positive enriched intestinal genes, intestine-enriched mRNA tag (Pauli), intestine enriched core and endoderm genes. Double listings were subsequently pruned. Gene ontology analyses were done with the help of the DAVID Bioinformatics Resources 6.8 tool (david.ncifcrf.gov, Huang et al., 2009a,b). Gene lists were submitted to the Gene ID Conversion Tool of DAVID and translated into corresponding Entrez Gene IDs. Genes not available in the DAVID database were manually converted. The resulting list was then resubmitted to the gene list manager and the selected species was set to *Caenorhabditis elegans*. Based on this list, a functional annotation chart was created using selection of GOTERM_BP_DIRECT, GOTERM_CC_DIRECT and GOTERM_MF_DIRECT with standard settings (Thresholds: Count=2 and EASE=0.1). The three complete lists of genes analyzed are provided in Tables S1-S3.

Analysis of larval development

A defined number of isolated embryos was placed onto each plate and incubated at 18°C. Hatched larvae were monitored every day for individuals reaching adulthood. The remaining larvae were transferred at least every 3 days. Larval arrest rates (%) were calculated from the ratios of animals dying as larvae and those reaching adulthood. Significance was determined using the chi-square test function of Excel. Time of larval development represents the average number of days animals needed to reach adulthood. Significance was calculated using the unpaired two-tailed *t*-test function of GraphPad Prism 5.01 (GraphPad Software Inc.).

Lifespan analysis

Isolated embryos were incubated at 18°C and vitality of hatched individuals was checked daily. We chose to incubate at 18°C as it is the optimal temperature for development of *ifo-1* mutants, which is otherwise perturbed. Animals were judged to be alive when they moved upon mechanical stimulation with a platinum wire. Hidden individuals were censored. Animals were transferred at least every 3 days to prevent mix-up with progeny. Statistical analysis was performed using the survival function and the Gehan–Breslow–Wilcoxon Test of GraphPad Prism 5.01.

Rescue experiments

Animals arrested at larval stages after 7 days of Cry5B intoxication were transferred onto plates with control JM103 bacteria for further incubation at 18°C. Animals reaching adulthood before death were counted as rescued. The rescue rate was calculated by determining the ratio of adult animals and the total number of viable larvae after 7 days of Cry5B treatment. Significance was determined using the chi-square test function of Excel.

Microscopy

Light microscopy was performed using either a confocal laser-scanning microscope (LSM 710, Zeiss) or a Zeiss Apotome fitted with a Zeiss AxioCamMRm. For electron microscopy, animals were cryofixed by rapid high-pressure freezing. To this end, animals were harvested and transferred into a 100 µm deep membrane carrier prefilled with 20% bovine serum albumin in M9 worm buffer (22 mM KH_2PO_4, 42 mM Na_2HPO_4, 86 mM NaCl, 1 mM $MgSO_4$) and high pressure frozen using a Leica EM Pact high-pressure freezer. At least five samples, each consisting of 10-20 worms, were fixed per experiment. Quick freeze substitution was applied using 1% OsO_4, 0.2% uranyl acetate in acetone followed by embedding into epoxy resin as previously described (McDonald and Webb, 2011). We prepared 50 nm transverse and longitudinal ultrathin sections with a Leica UC6/FC6 ultramicrotome, contrasted for 10 min each in 1% uranyl acetate in ethanol and Reynolds' lead citrate. Finally, sections were imaged at 100 kV using a Hitachi H-7600 transmission electron microscope.

Immunostaining and immunoblotting

Immunostaining was performed as previously described (Geisler et al., 2016). Mouse monoclonal anti-IFB-2 antibody (Developmental Studies Hybridoma Bank, MH33; Francis and Waterston, 1991) was used as primary diluted 1:100 in blocking solution [1% (w/v) nonfat milk powder (Carl Roth), 1% (w/v) bovine serum albumin (SERVA) and 0.02% (w/v) sodium azide] and Alexa Fluor 488-conjugated affinity-purified anti-mouse IgG (Invitrogen, A-11029; 1:200 in blocking solution) was used as secondary antibody. For quantification of immunostainings, intestines were isolated, stained against IFB-2 and subsequently imaged with a confocal laser-scanning microscope (LSM 710) using identical settings in a single session. Resulting stacks of individual intestines were then further processed using the sum-slice projection function of Fiji (fiji.sc). Intestines were manually defined as regions of interest and the average grayscale intensity per pixel was measured in this area using the measurement function of Fiji. Significance was evaluated using the unpaired, two-tailed *t*-test function of GraphPad Prism 5.01.

Immunoblotting and 2D gel electrophoresis assays were conducted as previously described (Geisler et al., 2016), with 60 worms per assay grown on control JM103 bacteria and 120 worms grown on Cry5B-producing JM103 bacteria. Primary antibodies against IFB-2 {MH33, Developmental Studies Hybridoma Bank, 1:1000 in blocking solution [1% (w/v) nonfat milk powder (Roth) or Roti®-Block (Roth) in case of 2D gel electrophoresis]} and actin (rabbit polyclonal antibodies, A2066, Sigma-Aldrich, 1:2000 in blocking solution) were used. Incubation with secondary antibodies [goat anti-mouse IgG antibodies and goat anti-rabbit IgG antibodies coupled to horseradish peroxidase (P0447 and P0448, respectively; Dako)] was performed at 1:7000 in blocking solution or Roti®-Block. For quantification of immunoblots chemiluminescent IFB-2 bands were measured using Fiji. Results were then normalized against the corresponding actin signal representing the protein loading control, which was further confirmed by Ponceau staining (Ponceau S solution, Sigma-Aldrich). Significance was evaluated using the unpaired, two-tailed *t*-test function of GraphPad Prism 5.01.

Acknowledgements

We thank Barbara Bonn for excellent technical support and Dr Nicole Schwarz for help with designing the CRISPR knockout constructs. We thank Drs Raffi Aroian (UMASS Medical School, MA, USA), Ralf Sommer (MPI, Tübingen, Germany), Christian Frøkjær-Jensen (University of Utah, USA) and Malene Hansen (Sanford Burnham Prebys Medical Discovery Institute, CA, USA) for valuable reagents. Some *C. elegans* and bacterial strains were provided by the *Caenorhabditis* Genetics Center (University of Minnesota, USA). Monoclonal antibody MH33 was obtained from the Developmental Studies Hybridoma Bank developed under the auspices of the National Institute of Child Health and Human Development and maintained by the University of Iowa, USA.

Competing interests

The authors declare no competing or financial interests.

Author contributions
Conceptualization: F.G., R.E.L.; Methodology: F.G., R.A.C., C.R., B.D.; Validation: F.G., R.A.C., C.R.; Formal analysis: F.G., R.A.C., C.R., B.D.; Investigation: F.G., R.A.C., C.R.; Resources: M.G., B.D., O.B., R.E.L.; Data curation: F.G., B.D.; Writing - original draft: F.G., R.E.L.; Writing - review & editing: F.G., R.E.L.; Visualization: F.G.; Supervision: F.G., R.E.L.; Project administration: R.E.L.; Funding acquisition: O.B., R.E.L.

Funding
The work was supported by a grant from the Deutsche Forschungsgemeinschaft (LE566/14-3 and BO1061/11-3).

Data availability
Transcriptome data have been deposited in Gene Expression Omnibus under accession number GSE125133.

Supplementary information
Supplementary information available online at
http://dev.biologists.org/lookup/doi/10.1242/dev.169482.supplemental

References

Alper, S., McBride, S. J., Lackford, B., Freedman, J. H. and Schwartz, D. A. (2007). Specificity and complexity of the Caenorhabditis elegans innate immune response. *Mol. Cell. Biol.* **27**, 5544-5553.
Asghar, M. N., Silvander, J. S. G., Helenius, T. O., Lahdeniemi, I. A. K., Alam, C., Fortelius, L. E., Holmsten, R. O. and Toivola, D. M. (2015). The amount of keratins matters for stress protection of the colonic epithelium. *PLoS ONE* **10**, e0127436.
Baugh, L. R. (2013). To grow or not to grow: nutritional control of development during Caenorhabditis elegans L1 arrest. *Genetics* **194**, 539-555.
Baumgart, D. C. and Dignass, A. U. (2002). Intestinal barrier function. *Curr. Opin Clin. Nutr. Metab. Care* **5**, 685-694.
Bement, W. M. and Mooseker, M. S. (1996). The cytoskeleton of the intestinal epithelium: Components, assembly, and dynamic rearrangements. In *The Cytoskeleton: A Multi-Volume Treatise*, Vol. 3 (ed. E. H. John and F. P. Ian), pp. 359-404. Greenwich; JAI Press.
Bischof, L. J., Huffman, D. L. and Aroian, R. V. (2006). Assays for toxicity studies in C. elegans with Bt crystal proteins. *Methods Mol. Biol.* **351**, 139-154.
Bolm, M., Jansen, W. T. M., Schnabel, R. and Chhatwal, G. S. (2004). Hydrogen peroxide-mediated killing of Caenorhabditis elegans: a common feature of different streptococcal species. *Infect. Immun.* **72**, 1192-1194.
Brown, D. T., Anderton, B. H. and Wylie, C. C. (1983). The organization of intermediate filaments in normal human colonic epithelium and colonic carcinoma cells. *Int. J. Cancer* **32**, 163-169.
Carberry, K., Wiesenfahrt, T., Windoffer, R., Bossinger, O. and Leube, R. E. (2009). Intermediate filaments in Caenorhabditis elegans. *Cell Motil. Cytoskeleton* **66**, 852-864.
Carberry, K., Wiesenfahrt, T., Geisler, F., Stocker, S., Gerhardus, H., Uberbach, D., Davis, W., Jorgensen, E., Leube, R. E. and Bossinger, O. (2012). The novel intestinal filament organizer IFO-1 contributes to epithelial integrity in concert with ERM-1 and DLG-1. *Development* **139**, 1851-1862.
Chelakkot, C., Ghim, J. and Ryu, S. H. (2018). Mechanisms regulating intestinal barrier integrity and its pathological implications. *Exp. Mol. Med.* **50**, 103.
Cho, S., Irianto, J. and Discher, D. E. (2017). Mechanosensing by the nucleus: from pathways to scaling relationships. *J. Cell Biol.* **216**, 305-315.
Coch, R. A. and Leube, R. E. (2016). Intermediate filaments and polarization in the intestinal epithelium. *Cells* **5**, 32.
Crawley, S. W., Mooseker, M. S. and Tyska, M. J. (2014). Shaping the intestinal brush border. *J. Cell Biol.* **207**, 441-451.
D'Alessandro, M., Russell, D., Morley, S. M., Davies, A. M. and Lane, E. B. (2002). Keratin mutations of epidermolysis bullosa simplex alter the kinetics of stress response to osmotic shock. *J. Cell Sci.* **115**, 4341-4351.
Darby, C. (2005). Interactions with microbial pathogens. *WormBook*, 1-15.
Estes, K. A., Szumowski, S. C. and Troemel, E. R. (2011). Non-lytic, actin-based exit of intracellular parasites from C. elegans intestinal cells. *PLoS Pathog.* **7**, e1002227.
Félix, M.-A., Ashe, A., Piffaretti, J., Wu, G., Nuez, I., Bélicard, T., Jiang, Y., Zhao, G., Franz, C. J., Goldstein, L. D. et al. (2011). Natural and experimental infection of Caenorhabditis nematodes by novel viruses related to nodaviruses. *PLoS Biol.* **9**, e1000586.
Francis, R. and Waterston, R. H. (1991). Muscle cell attachment in Caenorhabditis elegans. *J. Cell Biol.* **114**, 465-479.
Franke, W. W., Appelhans, B., Schmid, E., Freudenstein, C., Osborn, M. and Weber, K. (1979). The organization of cytokeratin filaments in the intestinal epithelium. *Eur. J. Cell Biol.* **19**, 255-268.
Frøkjær-Jensen, C., Davis, M. W., Hopkins, C. E., Newman, B. J., Thummel, J. M., Olesen, S.-P., Grunnet, M. and Jorgensen, E. M. (2008). Single-copy insertion of transgenes in Caenorhabditis elegans. *Nat. Genet.* **40**, 1375-1383.
Geisler, F. (2014). Identifizierung und Charakterisierung von intestinalen Zytoskelett-Organisatoren in Caenorhabditis elegans. *PhD thesis*, RWTH Aachen University, Aachen, Germany.
Geisler, F. and Leube, R. E. (2016). Epithelial intermediate filaments: guardians against microbial infection? *Cells* **5**, 29.
Geisler, F., Gerhardus, H., Carberry, K., Davis, W., Jorgensen, E., Richardson, C., Bossinger, O. and Leube, R. E. (2016). A novel function for the MAP kinase SMA-5 in intestinal tube stability. *Mol. Biol. Cell* **27**, 3855-3868.
Habtezion, A., Toivola, D. M., Butcher, E. C. and Omary, M. B. (2005). Keratin-8-deficient mice develop chronic spontaneous Th2 colitis amenable to antibiotic treatment. *J. Cell Sci.* **118**, 1971-1980.
Helenius, T. O., Antman, C. A., Asghar, M. N., Nyström, J. H. and Toivola, D. M. (2016). Keratins are altered in intestinal disease-related stress responses. *Cells* **5**, 35.
Hirokawa, N., Tilney, L. G., Fujiwara, K. and Heuser, J. E. (1982). Organization of actin, myosin, and intermediate filaments in the brush border of intestinal epithelial cells. *J. Cell Biol.* **94**, 425-443.
Huang, D. W., Sherman, B. T. and Lempicki, R. A. (2009a). Bioinformatics enrichment tools: paths toward the comprehensive functional analysis of large gene lists. *Nucleic Acids Res.* **37**, 1-13.
Huang, D. W., Sherman, B. T. and Lempicki, R. A. (2009b). Systematic and integrative analysis of large gene lists using DAVID bioinformatics resources. *Nat. Protoc.* **4**, 44-57.
Huffman, D. L., Abrami, L., Sasik, R., Corbeil, J., van der Goot, F. G. and Aroian, R. V. (2004). Mitogen-activated protein kinase pathways defend against bacterial pore-forming toxins. *Proc. Natl. Acad. Sci. USA* **101**, 10995-11000.
Hüsken, K., Wiesenfahrt, T., Abraham, C., Windoffer, R., Bossinger, O. and Leube, R. E. (2008). Maintenance of the intestinal tube in Caenorhabditis elegans: the role of the intermediate filament protein IFC-2. *Differentiation* **76**, 881-896.
Iatsenko, I., Sinha, A., Rödelsperger, C. and Sommer, R. J. (2013). New role for DCR-1/dicer in Caenorhabditis elegans innate immunity against the highly virulent bacterium Bacillus thuringiensis DB27. *Infect. Immun.* **81**, 3942-3957.
Jahnel, O., Hoffmann, B., Merkel, R., Bossinger, O. and Leube, R. E. (2016). Mechanical probing of the intermediate filament-rich Caenorhabditis elegans intestine. *Methods Enzymol.* **568**, 681-706.
Jaquemar, D., Kupriyanov, S., Wankell, M., Avis, J., Benirschke, K., Baribault, H. and Oshima, R. G. (2003). Keratin 8 protection of placental barrier function. *J. Cell Biol.* **161**, 749-756.
Kao, C.-Y., Los, F. C. O., Huffman, D. L., Wachi, S., Kloft, N., Husmann, M., Karabrahimi, V., Schwartz, J.-L., Bellier, A., Ha, C. et al. (2011). Global functional analyses of cellular responses to pore-forming toxins. *PLoS Pathog.* **7**, e1001314.
Kaplan, R. E. W., Chen, Y., Moore, B. T., Jordan, J. M., Maxwell, C. S., Schindler, A. J. and Baugh, L. R. (2015). dbl-1/TGF-beta and daf-12/NHR signaling mediate cell-nonautonomous effects of daf-16/FOXO on starvation-induced developmental arrest. *PLoS Genet.* **11**, e1005731.
Karabinos, A., Schünemann, J. and Parry, D. A. D. (2017). Assembly studies of six intestinal intermediate filament (IF) proteins B2, C1, C2, D1, D2, and E1 in the nematode C. elegans. *Cytoskeleton (Hoboken)* **74**, 107-113.
Kho, M. F., Bellier, A., Balasubramani, V., Hu, Y., Hsu, W., Nielsen-LeRoux, C., McGillivray, S. M., Nizet, V. and Aroian, R. V. (2011). The pore-forming protein Cry5B elicits the pathogenicity of Bacillus sp. against Caenorhabditis elegans. *PLoS ONE* **6**, e29122.
Kumar, V., Bouameur, J.-E., Bär, J., Rice, R. H., Hornig-Do, H.-T., Roop, D. R., Schwarz, N., Brodesser, S., Thiering, S., Leube, R. E. et al. (2015). A keratin scaffold regulates epidermal barrier formation, mitochondrial lipid composition, and activity. *J. Cell Biol.* **211**, 1057-1075.
Kumsta, C. and Hansen, M. (2012). C. elegans rrf-1 mutations maintain RNAi efficiency in the soma in addition to the germline. *PLoS ONE* **7**, e35428.
Lessard, J. C., Pina-Paz, S., Rotty, J. D., Hickerson, R. P., Kaspar, R. L., Balmain, A. and Coulombe, P. A. (2013). Keratin 16 regulates innate immunity in response to epidermal barrier breach. *Proc. Natl. Acad. Sci. USA* **110**, 19537-19542.
Lu, H., Chen, J., Planko, L., Zigrino, P., Klein-Hitpass, L. and Magin, T. M. (2007). Induction of inflammatory cytokines by a keratin mutation and their repression by a small molecule in a mouse model for EBS. *J. Invest. Dermatol.* **127**, 2781-2789.
MacQueen, A. J., Baggett, J. J., Perumov, N., Bauer, R. A., Januszewski, T., Schriefer, L. and Waddle, J. A. (2005). ACT-5 is an essential Caenorhabditis elegans actin required for intestinal microvilli formation. *Mol. Biol. Cell* **16**, 3247-3259.
Marroquin, L. D., Elyassnia, D., Griffitts, J. S., Feitelson, J. S. and Aroian, R. V. (2000). Bacillus thuringiensis (Bt) toxin susceptibility and isolation of resistance mutants in the nematode Caenorhabditis elegans. *Genetics* **155**, 1693-1699.
McDonald, K. L. and Webb, R. I. (2011). Freeze substitution in 3 hours or less. *J. Microsc.* **243**, 227-233.
Miller, E. V., Grandi, L. N., Giannini, J. A., Robinson, J. D. and Powell, J. R. (2015). The conserved G-protein coupled receptor FSHR-1 regulates protective host responses to infection and oxidative stress. *PLoS ONE* **10**, e0137403.

Munn, E. A. and Greenwood, C. A. (1984). The occurrence of submicrovillar endotube (Modified Terminal Web) and associated cytoskeletal structures in the intestinal epithelia of nematodes. *Philos. Trans. R. Soc. Lond. B Biol. Sci.* **306**, 1-18.
Owens, D. W. and Lane, E. B. (2003). The quest for the function of simple epithelial keratins. *BioEssays* **25**, 748-758.
Pekny, M. and Lane, E. B. (2007). Intermediate filaments and stress. *Exp. Cell Res.* **313**, 2244-2254.
Quinlan, R. A., Schwarz, N., Windoffer, R., Richardson, C., Hawkins, T., Broussard, J. A., Green, K. J. and Leube, R. E. (2017). A rim-and-spoke hypothesis to explain the biomechanical roles for cytoplasmic intermediate filament networks. *J. Cell Sci.* **130**, 3437-3445.
Rae, R., Iatsenko, I., Witte, H. and Sommer, R. J. (2010). A subset of naturally isolated Bacillus strains show extreme virulence to the free-living nematodes Caenorhabditis elegans and Pristionchus pacificus. *Environ. Microbiol.* **12**, 3007-3021.
Rae, R., Sinha, A. and Sommer, R. J. (2012). Genome-wide analysis of germline signaling genes regulating longevity and innate immunity in the nematode Pristionchus pacificus. *PLoS Pathog.* **8**, e1002864.
Roth, W., Kumar, V., Beer, H.-D., Richter, M., Wohlenberg, C., Reuter, U., Thiering, S., Staratschek-Jox, A., Hofmann, A., Kreusch, F. et al. (2012). Keratin 1 maintains skin integrity and participates in an inflammatory network in skin through interleukin-18. *J. Cell Sci.* **125**, 5269-5279.
Salas, P. J., Forteza, R. and Mashukova, A. (2016). Multiple roles for keratin intermediate filaments in the regulation of epithelial barrier function and apico-basal polarity. *Tissue barriers* **4**, e1178368.
Schwarz, N., Windoffer, R., Magin, T. M. and Leube, R. E. (2015). Dissection of keratin network formation, turnover and reorganization in living murine embryos. *Sci. Rep.* **5**, 9007.
Sem, X. H. and Rhen, M. (2012). Pathogenicity of Salmonella enterica in Caenorhabditis elegans relies on disseminated oxidative stress in the infected host. *PLoS ONE* **7**, e45417.
Senchuk, M. M., Dues, D. J. and Van Raamsdonk, J. M. (2017). Measuring oxidative stress in Caenorhabditis elegans: paraquat and juglone sensitivity assays. *Bio Protoc.* **7**, e2086.
Sifri, C. D., Begun, J. and Ausubel, F. M. (2005). The worm has turned–microbial virulence modeled in Caenorhabditis elegans. *Trends Microbiol.* **13**, 119-127.
Stutz, K., Kaech, A., Aebi, M., Kunzler, M. and Hengartner, M. O. (2015). Disruption of the C. elegans intestinal brush border by the fungal lectin CCL2 phenocopies dietary lectin toxicity in mammals. *PLoS ONE* **10**, e0129381.
Swift, J., Ivanovska, I. L., Buxboim, A., Harada, T., Dingal, P. C. D. P., Pinter, J., Pajerowski, J. D., Spinler, K. R., Shin, J.-W., Tewari, M. et al. (2013). Nuclear lamin-A scales with tissue stiffness and enhances matrix-directed differentiation. *Science* **341**, 1240104.
Tateishi, K., Nishida, T., Inoue, K. and Tsukita, S. (2017). Three-dimensional organization of layered apical cytoskeletal networks associated with mouse airway tissue development. *Sci. Rep.* **7**, 43783.
Treitz, C., Cassidy, L., Höckendorf, A., Leippe, M. and Tholey, A. (2015). Quantitative proteome analysis of Caenorhabditis elegans upon exposure to nematicidal Bacillus thuringiensis. *J. Proteomics* **113**, 337-350.
Troemel, E. R., Félix, M. A., Whiteman, N. K., Barrière, A. and Ausubel, F. M. (2008). Microsporidia are natural intracellular parasites of the nematode Caenorhabditis elegans. *PLoS Biol.* **6**, 2736-2752.
Turner, J. R. (2009). Intestinal mucosal barrier function in health and disease. *Nat. Rev. Immunol.* **9**, 799-809.
Veranič, P. and Jezernik, K. (2002). Trajectorial organisation of cytokeratins within the subapical region of umbrella cells. *Cell Motil. Cytoskeleton* **53**, 317-325.
Wang, L., Srinivasan, S., Theiss, A. L., Merlin, D. and Sitaraman, S. V. (2007). Interleukin-6 induces keratin expression in intestinal epithelial cells: potential role of keratin-8 in interleukin-6-induced barrier function alterations. *J. Biol. Chem.* **282**, 8219-8227.
Watanabe, N., Nagamatsu, Y., Gengyo-Ando, K., Mitani, S. and Ohshima, Y. (2005). Control of body size by SMA-5, a homolog of MAP kinase BMK1/ERK5, in C. elegans. *Development* **132**, 3175-3184.
Wei, J.-Z., Hale, K., Carta, L., Platzer, E., Wong, C., Fang, S.-C. and Aroian, R. V. (2003). Bacillus thuringiensis crystal proteins that target nematodes. *Proc. Natl. Acad. Sci. USA* **100**, 2760-2765.
Yang, W., Dierking, K. and Schulenburg, H. (2016). WormExp: a web-based application for a Caenorhabditis elegans-specific gene expression enrichment analysis. *Bioinformatics* **32**, 943-945.
Zupancic, T., Stojan, J., Lane, E. B., Komel, R., Bedina-Zavec, A. and Liovic, M. (2014). Intestinal cell barrier function in vitro is severely compromised by keratin 8 and 18 mutations identified in patients with inflammatory bowel disease. *PLoS ONE* **9**, e99398.

Supplementary Information

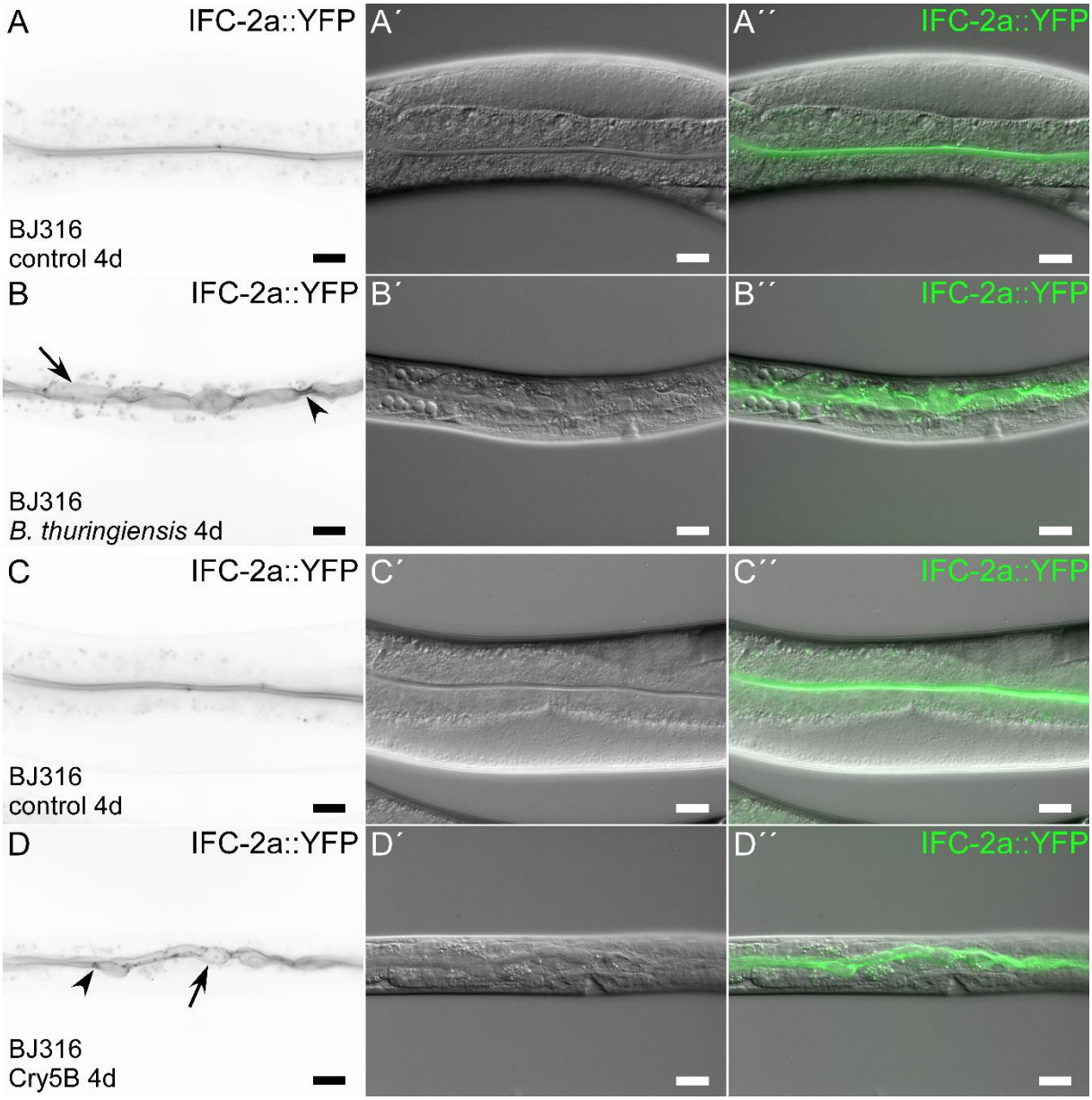

Fig. S1. IFC-2a::YFP redistributes upon infection with *Bacillus thuringiensis* or intoxication with Cry5B. The *in vivo* images show the distribution of the fluorescent IF protein IFC-2a::YFP that is produced from a *yfp*-tagged version of the endogenous *ifc-2a* gene (A-D; corresponding interference contrast images in A'-D'; merged images in A''-D''). Animals were grown for 4 days after hatching on OP50 (A-A''), *Bacillus thuringiensis* DB27 (B-B''), empty vector-containing control JM103 (C-C''), and Cry5B pore-forming toxin-producing JM103 (D-D''). Animals grown on control bacteria (OP50, control JM103) reach adulthood and display smooth periluminal localization of IFC-2a::YFP in the intestine (A-A'', C-C'') indistinguishable

from IFB-2a::CFP (Fig. 1C-C'', E-E'') indicating an intact intestinal lumen surrounded by a fully developed endotube. In contrast, infection with *Bacillus thuringiensis* DB27 (B-B'') or intoxication with its pore-forming toxin Cry5B (D-D'') induce intestinal lumen dilation and multiple cytoplasmic invaginations of the IF-rich endotube as also seen in the IFB-2a::CFP reporter strain (see Fig. 1D-D'', F-F''). Scale bars: 20 μm in A-D''.

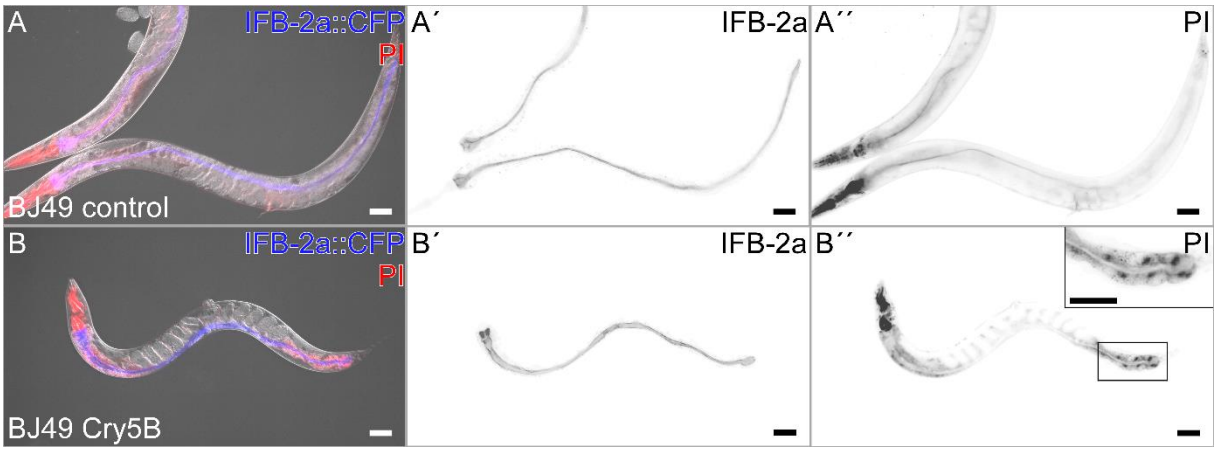

Fig. S2. The pore-forming toxin Cry5B induces pores at the apical plasma membrane of the intestinal cells without affecting junctional tightness. IFB-2a::CFP-producing reporter strain was first incubated either on control or on Cry5B-expressing JM103 for 24 hours. Animals were subsequently fed with the fluorescent tracer propidium iodide for 2 hours to assess intestinal integrity. The micrographs show that propidium iodide is retained in the intestinal lumen surrounded by a characteristic IFB-2a-positive endotube in the control (A-A'') but enters intestinal nuclei after Cry5B treatment, which has only elicited minor alterations in IFB-2a distribution at this time point (B-B''). Note that intercellular uptake of propidium iodide is not detectable indicating that the *C. elegans* apical junction is not affected by Cry5B intoxication. The uterine propidium iodide fluorescence in (A'' and B'') is caused by tracer uptake through the vulva. Scale bars: 50 µm.

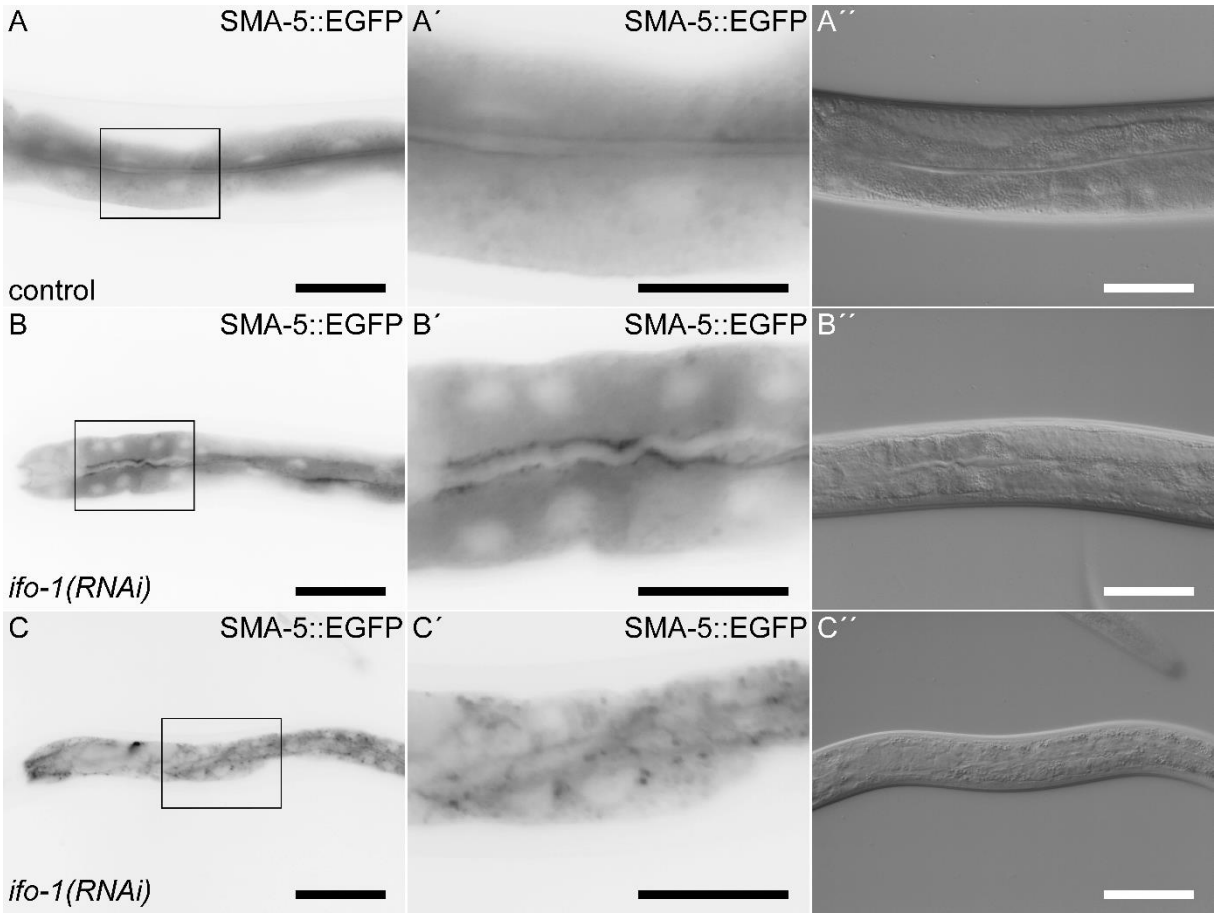

Fig. S3. SMA-5 accumulates apically and in cytoplasmic dots in *ifo-1(RNAi)* animals. The images (fluorescence micrographs in A-C with enlargements of boxed areas in A'-C' and corresponding interference contrasts in A''-C'') show that SMA-5::EGFP is uniformly localized in the intestinal cytoplasm and the apical plasma membrane of control animals (A-A'') but accumulates apically and in cytoplasmic dots in *ifo-1(RNAi)* intestines (B-C''). Note that the number of cytoplasmic dots appears to correlate with the strength of the RNAi-induced intestinal phenotype. Scale bar: 50 µm in A, A'', B, B'', C, C'', 25 µm in A', B', C'.

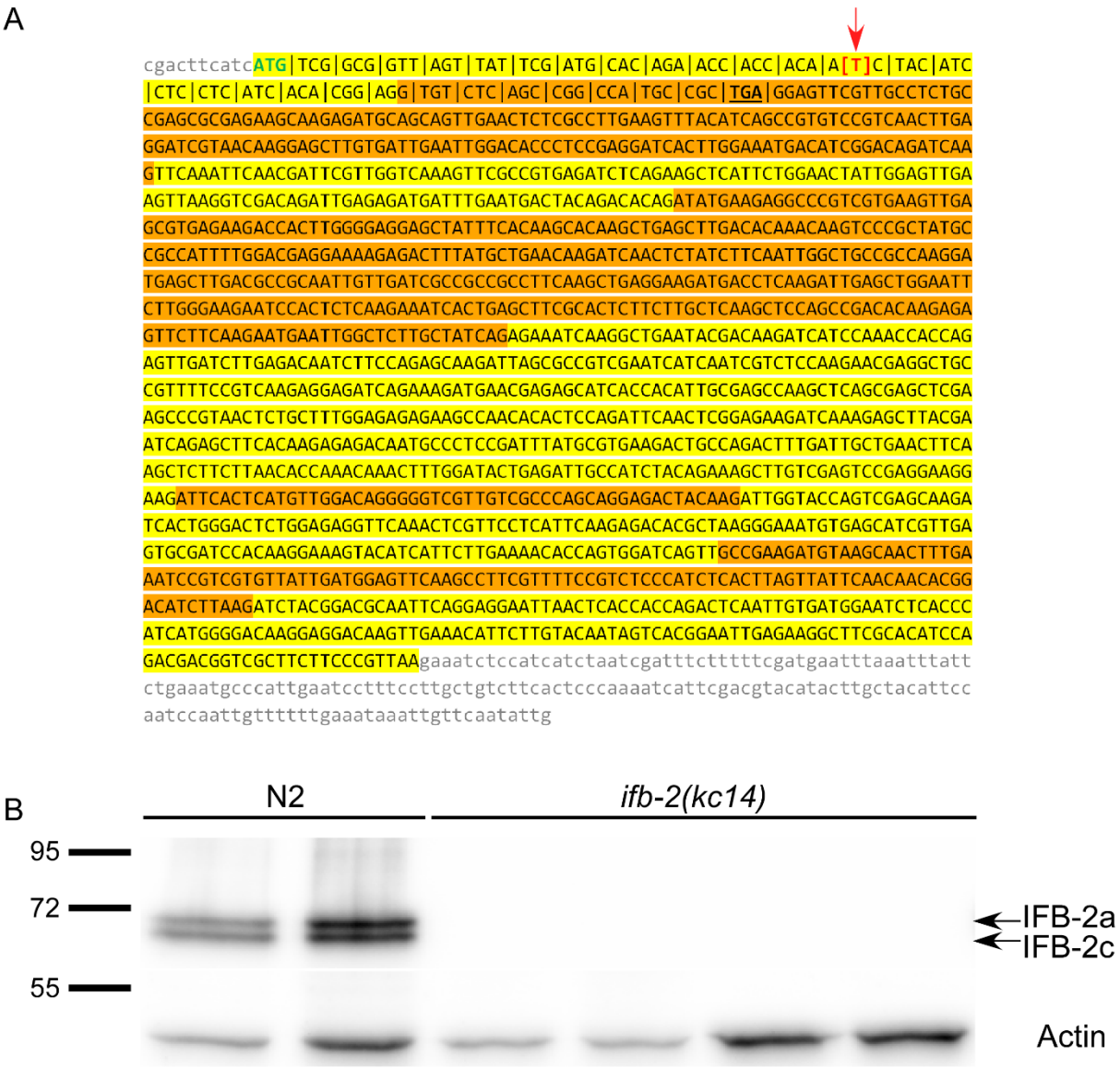

Fig. S4. Genetic alterations of allele *ifb-2(kc14)* and immunoblot analysis of whole worm lysates detecting IFB-2 and actin in N2 and *ifb-2(kc14)*. (A) shows the spliced gene model of *ifb-2* isoform a according to WormBase (www.wormbase.org; exons in alternating colors, non-translated region in grey letters, translational start codon in green). Mutant allele *ifb-2(kc14)* contains a thymidine insertion at position 41 (red arrrow) leading to a premature stop in the second exon (TGA in bold) resulting in a truncated 29 amino acid-long protein encompassing only 13 of the most aminoterminal amino acids of IFB-2a. The mutation also affects all other known IFB-2 isoforms, which share the same start codon and the aminoterminal part encoded by the first five exons. (B) The immunoblot shows complete absence of both IFB-2 isoforms a and c in worms harboring the *ifb-2* knockout allele *kc14*. The blot was subsequently incubated with pan-actin antibodies (lower panel). The position of co-electrophoresed size markers are shown in kDa at left.

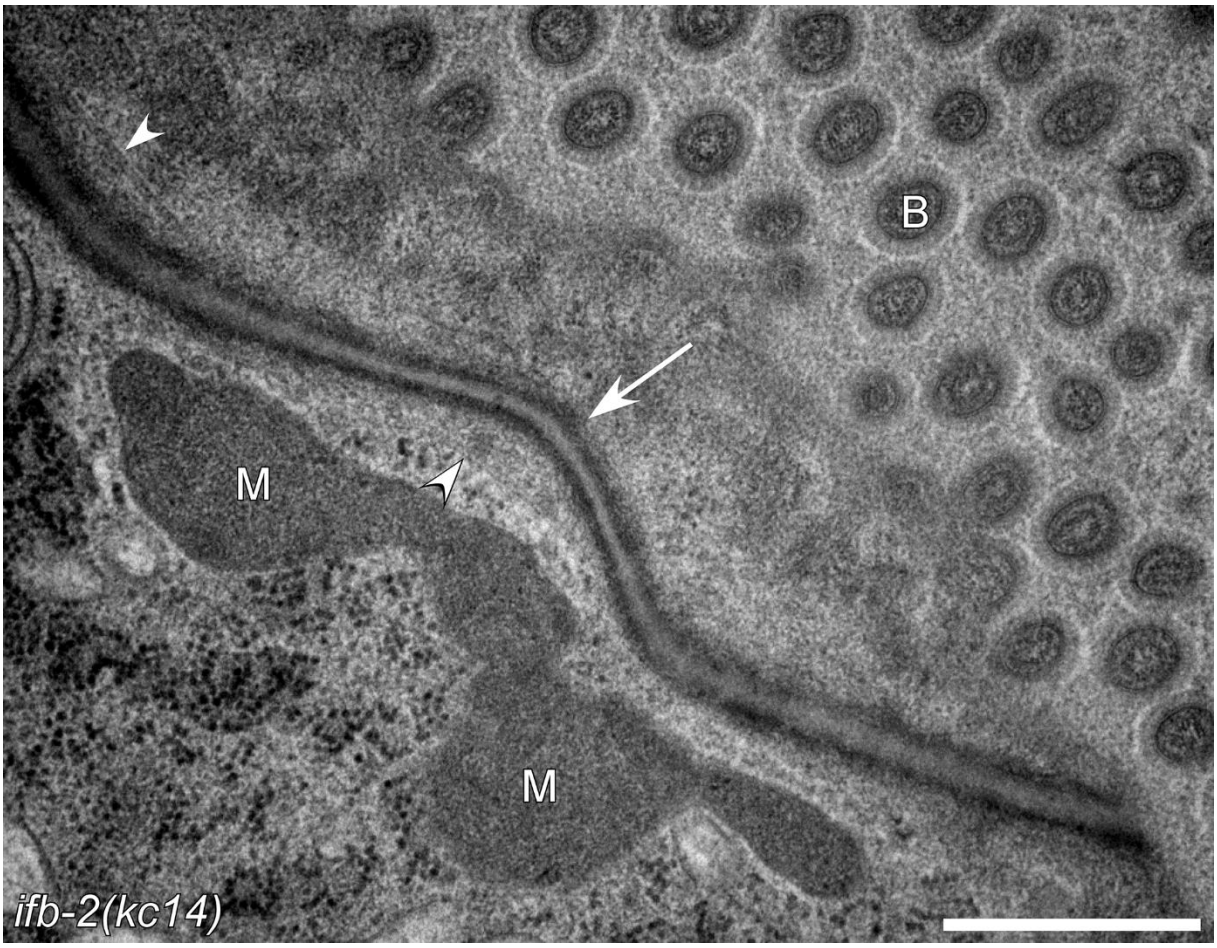

Fig. S5. The *C. elegans* apical junction lacks visible intermediate filaments in IFB-2 knockout animals. The electron micrograph is taken from a young adult *ifb-2(kc14)* knockout animal. The obliquely cut *C. elegans* apical junction appears to be unaffected (white arrow) except for a lack of associated IFs. Note multiple microtubules in close vicinity (white arrowheads). B, brush border; M, mitochondria. Scale bar: 500 nm.

Table S1. List of genes whose expression is either elevated or lowered in isolated intestines of *ifo-1(kc2)*. Transcriptome analyses were performed on intestines dissected from wild-type N2 and *ifo-1(kc2)* L4 mutants. RNA was prepared from 3 separate experiments for gene chip analysis. The list shows 808 upregulated and 256 downregulated genes (fold change >2; p-value <0.05).

Click here to download Table S1

Table S2. List of genes whose expression is either elevated or lowered upon Cry5B treatment in wild-type N2. Transcriptome analyses were performed in animals grown either on control JM103 or on Cry5B-producing JM103 for 4 days. RNA was prepared from 3 separate experiments for gene chip analysis. The list shows 1829 upregulated and 943 downregulated genes (fold change >2; p-value <0.05).

Click here to download Table S2

Table S3. List of genes whose expression is either elevated or lowered upon Cry5B treatment and mutation of the intestinal filament organizer IFO-1. Transcriptome analyses were performed to define similarities/differences of Cry5B intoxication and endotube impairment. RNA was extracted from N2 grown either on control JM103 or on Cry5B-producing JM103 for 4 days and from dissected intestines of adult wild-type and *ifo-1(kc2)*-mutant animals. RNA was extracted from 3 separate pools in each group for gene chip analysis. Comparison of the genes upregulated in both paradigms or downregulated in both paradigms identified 323 candidates (fold change >2; p-value <0.05).

Click here to download Table S3

Table S4. Ontology analysis of genes whose expression is either elevated or lowered by Cry5B treatment and by mutation of the intestinal filament organizer IFO-1. 54 genes are related to the innate immune response and 11 genes to the defense response to Gram-negative bacteria. Membrane rafts and extracellular space were the most affected cellular compartments, and carbohydrate binding was the most altered metabolic function.

Click here to download Table S4